Highlights

Online health-aware energy management strategy of a fuel cell hybrid autonomous mobile robot under startup-shutdown condition

Ghofrane Benarfa, Ali Amamou, Sousso Kelouwani, Marie Hébert, Lotfi Zeghmi, Samir Jemei

- Digital modeling and MDP to create diverse driving profiles for FCHAMR.
- Offline EMS with DP to balance FC degradation and hydrogen consumption.
- Transformer neural network to predict FC power trained by DP data.
- Online EMS with MPC to track optimal FC power obtained by prediction from Transformer network.

Ghofrane Benarfa^{a,*,1}, Ali Amamou^a, Sousso Kelouwani^b, Marie Hébert^b, Lotfi Zeghmi^a and Samir Jemei^c

ARTICLE INFO

Keywords: Industry 4.0 Autonomous mobile robot Energy management strategy Transformer neural network digital Model Predictive Control

ABSTRACT

In the age of Industry 4.0, the automation of industrial processes is essential for enhancing efficiency, productivity, and flexibility. Autonomous mobile robots are pivotal in this transformation, particularly in material handling and logistics operations within complex industrial environments. Fuel cell hybrid autonomous mobile robots, a type of autonomous mobile robot that functions with hybridization of battery and fuel cell, offer significant advantages in operational efficiency and sustainability. However, the commercialization of these vehicles is impeded by the limited lifespan of fuel cells and the adverse effects of frequent startup-shutdown cycles, which lead to significant fuel cell degradation and reduced operational efficiency. This study addresses these challenges by presenting an innovative, health-aware energy management strategy tailored for fuel cell hybrid autonomous mobile robots. The proposed strategy aims to balance hydrogen consumption with fuel cell degradation through a comprehensive two-step approach. First, the offline phase employs digital modeling combined with a Markov Decision Process to generate long-term power profiles. This step includes the use of Dynamic Programming to optimize power distribution, ensuring an efficient energy management strategy. Additionally, a transformer neural network is trained on this optimized data to accurately predict the fuel cell's power output. In the online step, a Model Predictive Control technique is utilized to dynamically track the fuel cell's power output based on real-time predictions from the trained transformer model. This enables the system to adapt to changing operational conditions, maintaining optimal performance and extending the fuel cell's lifespan. Our comparative analysis, based on simulations and experimental tests conducted in a controlled laboratory environment, demonstrates that this approach enhances both fuel cell lifespan and hydrogen efficiency. Specifically, our strategy extends the fuel cell's operational life by 9.5% and achieves a hydrogen consumption of 15.83 grams over a 600-second operational cycle, compared to benchmark methods. The novelty of this research lies in its integration of advanced predictive models and control techniques, which collectively optimize the operational efficiency and durability of fuel cell hybrid autonomous mobile robots.

1. Introduction

1.1. Motivation

In the era of Industry 4.0, the automation of industrial processes has become a pivotal aspect for enhancing efficiency, productivity, and flexibility. Autonomous Mobile Robots (AMRs) have emerged as key players in this paradigm, revolutionizing material handling and logistics operations within indoor environments (Mohammadpour et al., 2022). These AMRs are designed to navigate and transport goods, eliminating the need for manual intervention and streamlining operations. Efficient navigation is crucial for AMRs to perform their tasks effectively within the confines of industrial settings. Unlike traditional outdoor vehicles that operate in open spaces, AMRs encounter a controlled and structured environment, characterized by narrow aisles, congested pathways, and potential obstacles

^aDepartment of Electrical and Computer Engineering, Hydrogen Research Institute, University of Québec at Trois-Rivières, Trois-Rivières, G8Z 4M3. OC. Canada

^bDepartment of Mechanical Engineering, Hydrogen Research Institute, University of Québec at Trois-Rivières, Trois-Rivières, G8Z 4M3, OC, Canada

^cUniversité de Franche-Comté, UTBM, CNRS, FEMTO-ST, FCLAB, Belfort, 25030 CEDEX, France

^{*} This work was supported by the Industrial Research Chair Noovelia and by the Natural Science and Engineering Research Council of Canada.

^{*}Corresponding author

ghofrane.benarfa@uqtr.ca(G. Benarfa); ali.amamou@uqtr.ca(A. Amamou); sousso.kelouwani@uqtr.ca(S. Kelouwani); marie.hebert@uqtr.ca(M. Hébert); lotfi.zeghmi@uqtr.ca(L. Zeghmi); samir.jemei@univ-fcomte.fr(S. Jemei)
ORCID(s): 0009-0007-2402-1593(G. Benarfa)

such as machinery, equipment, and human workers (Tian et al., 2024). In navigating these complex environments, AMRs rely on two essential components: the local planner and the global planner. The local planner handles real-time obstacle avoidance and immediate path planning, ensuring safe and efficient navigation through dynamic and congested areas. Meanwhile, the global planner is responsible for determining the optimal path from start to destination, taking into account factors such as distance, time, and energy efficiency. This dual-planning approach allows AMRs to dynamically adapt to immediate environment changes while maintaining an overall efficient route.

Significant research has focused on improving the intelligence of AMRs in complex environments in planning, navigation, mapping, scheduling, fleet management, etc. (Madridano et al., 2021), yet energy management has not been extensively studied for these vehicles, leaving a significant gap in understanding and development in this critical area. AMRs frequently use batteries as their main source of energy. Battery-powered AMRs provide substantial benefits in terms of sustainability and minimizing environmental impact in indoor settings. By utilizing onboard batteries, these vehicles eliminate emissions associated with traditional fuel-powered vehicles and offer the additional advantage of quieter operation. However, battery-powered AMRs face challenges regarding limited battery life, and necessitate frequent recharging which may result in operational downtime (Graba et al., 2023). Alternatively, fuel cell (FC)-based AMRs present a promising solution to overcome the limitations of battery-powered systems (Cheng et al., 2022; Poonthalir & Nadarajan, 2019; Wu et al., 2023). These vehicles offer extended operating times and can quickly refuel by replacing the FC tanks (Farooq et al., 2023). However, FC-powered AMRs also face certain limitations, such as slower dynamic performance, limited power density, inefficiency at low loads, limited cold start capability, and FC degradation (Tsalapati et al., 2021).

Considering the advantages and disadvantages of both battery-powered and FC-based AMRs, hybridization emerges as a practical approach. FC hybrid AMRs (FCHAMRs) combine the benefits of both battery and FC systems, allowing for optimized energy utilization and prolonged operation within industrial settings (Ehsani et al., 2018). To efficiently distribute power between these resources, hybrid systems require the presence of an energy management strategy (EMS). The EMS plays a crucial role in managing the power flow between the battery and FC, ensuring that each component operates within its optimal range. This strategic distribution not only enhances the overall efficiency and reliability of the AMR but also extends the operational time, making FCHAMRs particularly well-suited for demanding industrial environments.

However, despite these advantages, FCHAMRs still encounter significant challenges, particularly in their energy efficiency and the degradation of their energy sources (Ghobadpour et al., 2020). Moreover, enhancing the energy efficiency of the FCHAMR and ensuring the long-term durability of the FC are especially critical in dynamic environments. These environments are characterized by operational constraints, workload variations, and diverse mission requirements. In such settings, the vehicles are required to start and stop multiple times during operations. The frequent cycling (startup-shutdown) of FCs in these conditions leads to heightened mechanical, thermal, and water management stresses, that negatively impact the FC's efficiency, lifespan, and overall performance. Figure 1 illustrates these environmental challenges, including high collision risks, dynamic obstacles, continuous operations, and varied loads, which collectively cause rapid fluctuations in power demand and contribute to excessive startup-shutdown cycles, accelerating FC degradation.

Addressing the degradation issue within the EMS is essential for ensuring the seamless and prolonged functioning of FCHAMRs in such demanding operational environments. The EMS must be capable of managing these stresses effectively to sustain the longevity of the FC while optimizing the energy efficiency of the system. This involves developing sophisticated algorithms and control strategies that can dynamically adjust to the varying operational conditions, workload demands, and mission profiles of the AMR. The core research question is how to sustain the longevity of the FC and optimize the energy efficiency of the system, all within the constraints of a dynamic environment.

1.2. Related work

Energy management for FCHAMRs is still a relatively unexplored field, mainly due to the distinct challenges presented by their dynamic operational environments. On the other hand, many EMSs have been developed for outdoor FC hybrid electric vehicles (FCHEVs) to efficiently manage power distribution between the battery and the FC (Eckert, Barbosa, Silva, Roso, Silva, & da Silva, 2022). To effectively explore and develop EMS for FCHAMRs, it is crucial to examine these established EMSs for FCHEVs. Indeed, these EMSs can be broadly classified into rule-based, optimization-based and data-based strategies (Zhao et al., 2022). A health-aware rule-based EMS consists of rules designed based on human expertise to find efficient operating points that mitigate energy source degradation.

High risk of collision High presence of dynamic obstacles Continuous long term operations Variations of loads and missions

- X Rapid fluctuations in speed and power demand
- X Frequent startup/shutdown cycles of the FC: accelerated FC degradation

Figure 1: industrial environment challenges

Rule-based EMSs are classified into two categories: deterministic and fuzzy strategies. Deterministic strategies, such as the thermostat, frequency split, and state machine strategies, are practical for achieving multiple objectives, like reducing system degradation and fuel consumption (Bayindir et al., 2011; Meintz & Ferdowsi, 2008). For example, frequency split EMS decomposes power demand into frequency bands to ensure the FC operates within acceptable ranges (Ibrahim et al., 2014). However, these methods lack flexibility and fail to obtain general solutions. Fuzzy rule-based strategies use fuzzy inference systems to convert inputs and outputs into linguistic terms, which are then defuzzified into control signals (Eckert, Barbosa, Silva, Roso, Silva, & Da Silva, 2022; Yavuz et al., 2015). For instance, Ravey et al. used the FC degradation index as an input to a fuzzy logic controller to manage FC degradation (Ravey et al., 2015). Martinez et al. combined expert insights using a Type-2 fuzzy system to handle rule uncertainties, controlling FC reference current to meet power demand and maintain battery SoC (Martínez et al., 2013a). Despite their ease of implementation, fuzzy strategies struggle to achieve optimality. In summary, rule-based strategies are easy to design and implement for real-time FCHEV applications but achieving optimality is challenging.

Therefore, optimization-based strategies are introduced and are often classified into global offline optimization and real-time optimization strategies (Ravey et al., 2012). Global offline optimization strategies aim to find the optimal solution by solving a health-aware cost function, but rely on the entire driving cycle (Li et al., 2020; Sulaiman et al., 2018). For example, Dynamic Programming (DP) divides the optimization problem into sub-problems and calculates the cost function for each discrete time step, finding the minimum cost path (Xu et al., 2012). DP was utilized in minimizing FC degradation, battery degradation, hydrogen consumption, and recharging costs. However, DP is sensitive to driving cycles and computationally heavy. Additionally, DP can be a tool for evaluation and comparison, generating data to train artificial neural networks for real-time near-optimal results. Stochastic search methods, such as genetic algorithms (Jordán et al., 2022), particle swarm optimization (PSO) (Sarma & Ganguly, 2020), and simulated annealing, are effective for multi-objective problems. These methods iteratively solve optimization problems, like the multi-objective fitness function considering FC cost, capacity cost, and total energy cost (Herrera et al., 2016). However, these methods are also cycle-sensitive and require predefined driving conditions. Consequently, real-time optimization methods have been introduced to provide reactive and real-time control, ensuring efficient and adaptive performance in varying operational conditions. Real-time optimization strategies, such as Equivalent Consumption Minimization Strategy (ECMS) and Equivalent Degradation Minimization Strategy (EDMS), minimize a real-time cost function (Zeng et al., 2021), often using Pontryagin's Minimum Principle (PMP) for constrained optimization (Liu & Liu, 2015). Model Predictive Control (MPC) is another real-time optimization approach that solves the optimization problem at each sampling instant, involving multiple constraints in control actions (Y. Zhou et al., 2021). MPC has been used to meet power demands and set battery SoC constraints to prevent degradation, reducing computational costs compared to PMP and DP while handling moving horizons (Arce et al., 2009). He et al. propose a costminimizing MPC-based power allocation technique for FC/battery hybrid buses, integrating FC lifespan and battery aging models to balance hydrogen consumption and durability, and enhancing speed forecast accuracy (Martínez et al., 2013b). Although MPC solutions are typically sub-optimal, combining dynamic programming can enhance real-time decision-making and health management efficiency. Moreover, Adaptive Dynamic Programming (ADP)

(Stojanović, 2023) can be utilized in EMS both offline and online; however, it often encounters challenges related to computational efficiency, scalability, and convergence. Feedback-aided PD-type iterative learning control has been used in EMS to iteratively optimize power distribution strategies by learning from historical data and previous operational cycles, thereby improving accuracy and adaptability in dynamic and time-varying environments (Guan et al., 2023). Additionally, composite adaptive finite-time fuzzy control (Sun et al., 2023) has been applied in EMS to achieve robust and efficient energy management under varying and complex conditions, ensuring optimal performance despite dynamic environmental changes. While optimization-based methods have proven effective in EMS, they are inherently limited by random and model uncertainties. These uncertainties can impact the reliability of model predictions, as real-world operational conditions often deviate from the predefined scenarios assumed during the optimization process. Model uncertainties arise from simplifications or assumptions within the system's mathematical representation, potentially leading to discrepancies between predicted and actual system behavior. Similarly, random uncertainties, due to unpredictable fluctuations in environmental and operational factors, introduce variability that these methods cannot fully account for. Consequently, these factors can affect the consistency and robustness of optimization outcomes, especially in dynamic environments where the EMS must continuously adapt to changing demands. Addressing these uncertainties is critical for advancing EMS reliability and robustness in practical applications (Bomze & Gabl, 2023).

Data-based methods, known as intelligent control strategies, are well-suited for solving complex problems and are widely used in EMS development (W. Chen et al., 2023; Huang et al., 2023; Vichard et al., 2020; X. Wang et al., 2020). Various machine learning strategies, including neural networks (Z. Chen et al., 2013; Ming et al., 2023), support vector regression (SVR) (Montero-Sousa et al., 2020), are documented in the literature. Song et al. propose a degradation-adaptive EMS that dynamically adjusts power distribution based on the FC's state-of-health (Song et al., 2021). Using a novel degradation model, the EMS optimizes control to enhance energy efficiency and ensure realworld feasibility. Q-learning (Fayyazi et al., 2023; R. Wang et al., 2023) has also been extensively used in EMS for health-aware control, optimizing performance by learning from historical data and adapting to changing conditions. Reinforcement learning (RL) has been widely applied in EMS. Hu et al., 2023) propose a power distribution optimization strategy for FCHEVs using deep reinforcement learning (DRL) and PMP to balance fuel economy, battery durability, and FC durability, demonstrating significant reductions in degradation. However, machine learning methods face practicality issues due to the heavy computational load of training datasets. Further methods, such as targeted transfer learning through distribution barycenter medium (TTL-DBM) (Yang, Lei, Li, & Li, 2024), a federated learning approach that facilitates decentralized data use without central storage, and label recovery and trajectory designable network (LRTDN) (Yang, Lei, Li, Li, & Nandi, 2024), a model addressing label inconsistencies across domains, provide advanced solutions for fault diagnosis. However, even with these advancements, they remain insufficient for fully addressing the complex, real-time demands of EMS in dynamic environments. Furthermore, remote structural health monitoring approaches, such as those using satellite sensing in outdoor infrastructure settings, present an interesting perspective on managing structural health and risk in complex systems. For example, a recent study applied remote sensing and GIS-based monitoring to urban infrastructure to assess risk and coordinate management strategies across connected road systems (Troisi & Castaldo, 2022). Although primarily relevant to large-scale outdoor applications, such techniques emphasize the potential of remote monitoring to enhance real-time decision-making.

A significant amount of research has been devoted to developing health-aware EMS for FCHEVs used in outdoor applications. However, there has been less effort in the realm of FCHAMRs. Although FCHAMRs share similarities with FCHEVs, they also have crucial differences, making the direct application of FCHEV algorithms challenging. Unlike outdoor FCHEVs, FCHAMRs operate in dynamic environments marked by frequent obstacles and the need for rapid trajectory adjustments. This dynamic nature necessitates continuous modifications to FCHAMR trajectories, leading to multiple start-stop cycles for the FC. These repetitive cycles heavily impact FC efficiency and overall lifespan, with start-stop degradation becoming more pronounced. Moreover, the dynamic environment causes instantaneous changes in energy demand, measured in milliseconds, due to abrupt shifts in task requirements and workload variations. Such rapid and unpredictable energy needs make it difficult for EMS to keep pace and make precise real-time decisions. Consequently, there are several significant gaps in the research focusing on health-aware energy management for FCHAMRs:

- There is a significant shortage of detailed and comprehensive datasets reflecting the specific operational conditions of FCHAMRs, which hampers the development of robust EMS.
- Existing EMS algorithms are not equipped to handle the high level of adaptability required for FCHAMRs in dynamic environments with instantaneous energy demand fluctuations.

• There is a lack of EMS specifically designed to mitigate the negative impact of frequent start-stop cycles on the FC's efficiency and durability.

These gaps highlight the urgent need for tailored approaches that address the specific challenges and requirements in industrial environments, emphasizing the importance of health-aware energy management and start-stop degradation mitigation for FCHAMRs.

1.3. Contribution and organisation

Inspired by the logic of global and local planning in navigation, this article proposes a two-step EMS framework that offers a compromise between FC degradation due to startup-shutdown cycles, battery efficiency, and hydrogen consumption. It comprises two key steps: First, an offline FC health-aware EMS, which operates similarly to the global planner. This EMS analyzes vast datasets and derives optimal, static solutions based on data created through simulations with digital modeling and Markov Decision Process (MDP). This step creates a comprehensive EMS considering all possible scenarios, and the output of the DP becomes the training ground for a Transformer neural network, enabling precise FC power predictions. Second, an online EMS based on MPC operates like the local planner. The trained Transformer model receives real-time data from the FCHAMR's local planner and energy model, then makes predictions about the power of the FC in a specific window. The MPC tracks the predicted FC power while using information from the FCHAMR's sensors and environment to adjust the EMS. By leveraging this two-module approach, the proposed EMS framework seeks to optimize energy management for improved performance in FCHAMRs, ensuring rapid system response.

According to the above discussion, the EMS proposed in this paper has three major contributions that highlight the novelty and the relevance of the study:

- Developing methods to generate and utilize detailed and comprehensive datasets that reflect the specific
 operational conditions of FCHAMRs. This is facilitated through the introduction of a generative digital
 modeling-MDP approach, enabling rapid generation of diverse requested power profiles for FCHAMR and
 eliminating the need for extensive manual data collection in industrial settings.
- Balancing hydrogen consumption and FC degradation induced by recurrent startup-shutdown cycles, ensuring
 the longevity of the FC as well as the energy efficiency of the system, in dynamic industrial environments. This
 contribution is introduced through the first step of the EMS including the optimal offline power distribution with
 DP.
- Handling the high level of adaptability required for FCHAMRs by using an online MPC based EMS with input
 from Transformer neural network power prediction, adaptive to real-time adjustments. This step allows the EMS
 to effectively respond to instantaneous energy demand fluctuations in dynamic and unpredictable environments.

The rest of the paper is organized as follows. Section 2 describes the FC-battery hybrid system of FCHAMR in detail. Section 3 describes the energy management strategy with FC health-aware control. Section 4 describes the benchmarking strategies used to evaluate the proposed methodology and discusses the results. Section 5 summarizes the conclusions and future challenges.

2. System description

This study utilizes a FCHAMR designed for industrial warehouse applications. Each driving wheel of the FCHAMR is equipped with a brushless motor that features a single speed gearbox. To ensure balance, the aluminum body frame is equipped with four castor wheels. Figure 2 shows the studied FCHAMR.

2.1. Hybrid powertrain model

The FCHAMR effects different set of tasks inside the warehouse under certain conditions and parameters: The linear and angular velocities remain relatively constant over time. Table 1 shows the parameters' values of the studied vehicle.

Figure 3 shows the powertrain structure that comprises a 500-W Proton exchange membrane fuel cell (PEMFC) and a Lithium battery pack.

In this modeling of the FCHAMR's hybrid powertrain system, several assumptions were made to simplify the analysis and focus on the key performance aspects:

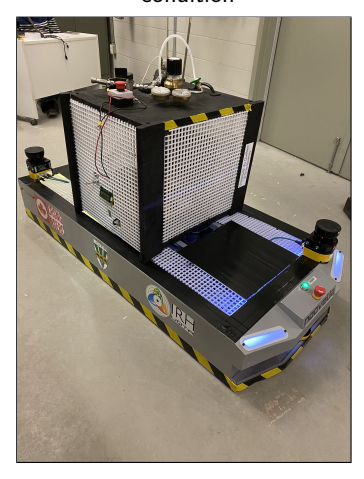


Figure 2: The studied FCHAMR in the laboratory

Table 1Technical characteristics of the studied FCHAMR

Parameter	Value
Maximum speed	1m/s
Maximum acceleration	$0.08 \ m/s^2$
Maximum load	1000 Kg
FCHAMR mass	100 Kg
Overall dimensions	$L = 1.65 \text{ m} \mid W = 0.72 \text{ m} \mid H 0.25 \text{m}$
Battery	24 V, 40 Ah
FC power	500 W
FC auxiliaries	No compressors (open cathode FC), 5.2 L H_2 tank, valves, pipe, fan for cooling and air supply
Motors	Brushless (BLDC)

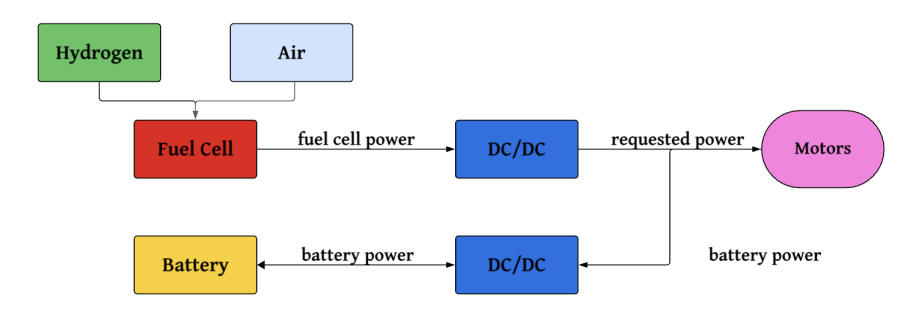


Figure 3: Parallel configuration of the FCHAMR

- The FCHAMR operates 24 hours a day, 5 days a week.
- The linear and angular velocities of the FCHAMR remain relatively constant over time.
- Air resistance and aerodynamic drag forces are negligible.
- The coefficient of rolling friction (μ) between the wheels and the ground is constant.
- The mass of the FCHAMR is uniformly distributed.
- The power consumption of auxiliary electronics (sensors, computer, etc.) is constant over time.

- The efficiencies of the motors (η_{mot}) , transmission (η_{tr}) , and DC/AC converter (η_{cont}) are constant.
- The voltage reference and current draw for the auxiliary systems are constant.

The energy model of the FCHAMR can be expressed as Eq. 1:

$$E_{FCHAMR} = E_{motors} + E_{kinetic} + E_{friction} + E_{aux} \tag{1}$$

Where $E_{FCHAMR}(Wh)$ represents the total requested energy for the FCHAMR, $E_{motors}(Wh)$ is the energy requested by the motors, $E_{kinetic}(Wh)$ accounts for the kinetic energy, $E_{friction}(Wh)$ refers to the rolling friction energy of the FCHAMR wheels with the ground, and $E_{aux}(Wh)$ denotes the energy from the auxiliary electronics in the FCHAMR, such as the computer and different sensors.

Firstly, the auxiliary electronics' energy is modeled. It is represented by Eq. 2:

$$E_{aux} = \int \left(V_{ref} I_{aux} \right) dt \tag{2}$$

Where $I_{aux}(A)$ denotes the amount of current withdrawn by the auxiliary components, and $V_{ref}(V)$ represents the nominal reference voltage of the FCHAMR.

Furthermore, the rolling friction energy is incorporated into the model, and its calculation is detailed by equations (3-6):

$$P_{friction}^{R} = \mu mg(v(t) + b\omega(t)) \tag{3}$$

$$P_{friction}^{L} = \mu mg(v(t) - b\omega(t)) \tag{4}$$

$$P_{friction} = P_{friction}^{R} + P_{friction}^{L} \tag{5}$$

$$E_{friction} = \int P_{friction} dt \tag{6}$$

Here, $P_{friction}^R(W)$ and $P_{friction}^L(W)$ are the rolling friction power for the right and left wheels, $P_{friction}(W)$ is the total rolling friction power, μ represents the coefficient of rolling friction, m(Kg) is the total mass of the FCHAMR, $g(m/s^2)$ is the gravitational constant, b(m) denotes the axial length of the FCHAMR with a parallelepiped shape, while v(m/s) and $\omega(rad/s)$ respectively denote the linear and angular velocities of the FCHAMR's center of mass. These velocities can be obtained from the FCHAMR kinematics model. Eq. 7a and Eq. 7b illustrate how to calculate the linear and angular velocities of the FCHAMR (v and v) based on the angular velocities of the wheels, which are measured by odometry sensors:

$$v = \frac{r}{2(\omega^R + \omega^L)} \tag{7a}$$

$$\omega = \frac{r}{2b(\omega^R - \omega^L)} \tag{7b}$$

In these equations, r(m) refers to the radius of the FCHAMR's driving wheel, and $\omega^R(rad/s)$ and $\omega^L(rad/s)$ represent the rotational velocities of the wheels.

Thirdly, the kinetic energy is analyzed and modeled through equations 8a and 8b:

$$E_{kinetic} = \frac{1}{2} \left(mv(t)^2 + I\omega(t)^2 \right) \tag{8a}$$

$$I = \frac{1}{12}m\left(a^2 + (2b)^2\right) \tag{8b}$$

Where $I(Kg.m^2)$ represents the inertia of the FCHAMR, and a(m) denotes the geometric length of the FCHAMR with a parallelepiped shape.

Finally, the motors' power $P_m^R(W)$ and $P_m^L(W)$ is characterized using equations 9a and 9b for the mechanical power of the brushless motors:

$$P_m^R = \frac{(T^R \omega_m^R)}{\eta_{mot} \eta_{tr} \eta_{cont}} \tag{9a}$$

$$P_m^L = \frac{(T^L \omega_m^L)}{\eta_{mot} \eta_{tr} \eta_{cont}} \tag{9b}$$

Here, η_{mot} , η_{tr} and η_{cont} respectively represent the efficiencies of the motors, transmission system, and the DC/AC converter. $T^R(Nm)$ and $T^L(Nm)$ signify the torque applied to the right and left motors, while ω_m^R (rad/s) and ω_m^L (rad/s) refer to the angular velocities of the right and left motors, calculated by Eq. 10a and Eq. 10b:

$$\omega_m^R = N_{tr} \omega^R \tag{10a}$$

$$\omega_m^L = N_{tr} \omega^L \tag{10b}$$

Where N_{tr} is the transmission ratio of the transmission system. The torque forces T^R and T^L are presented by equations 11a and 11b, respectively:

$$T^R = r \cdot F^R \tag{11a}$$

$$T^L = r \cdot F^L \tag{11b}$$

Here, $F^R(N)$ and $F^L(N)$ represent the forces applied to each wheel. These forces can be calculated from the traction force F(N) and the rotation angle $\theta(rad)$ of the FCHAMR using Eq. 12:

$$F^R = F^L = \frac{1}{2} \frac{F}{\cos(\theta)} \tag{12}$$

The traction force F of the FCHAMR can be determined assuming both α and $F_{aero}(N)$ to be null (applicable to indoor flat surface scenarios) calculated in Eq. 13a-13d:

$$m\frac{dv}{dt} = F - F_{res} \tag{13a}$$

$$F_{res} = F_r + F_{aero} + mg\sin(\alpha) \tag{13b}$$

$$F_r = mg\mu\cos(\alpha) \tag{13c}$$

$$F = m\frac{dv}{dt} + mg\mu \tag{13d}$$

In summary, the power of the motors $(P_{motors}(W))$ and the energy consumed by the motors $(E_{motors}(Wh))$ are obtained through equations 14a and 14b:

$$P_{motors} = P_m^R + P_m^L \tag{14a}$$

$$E_{motors} = \int P_{motors} dt \tag{14b}$$

Table 2 presents all the constants that have been used in equations (1-13d).

Table 2
Technical characteristics of the studied FCHAMR

Constant	Value	Description
r	0.096 m	Wheel's radius
b	0.72 m	Axial length
$\eta_{ m mot}$	0.9	Motor's efficiency
η_{tr}	0.93	Transmission's efficiency
$\eta_{ m cont}$	0.9	Controller's efficiency
N_{tr}	1	Transmission's ratio
g	$9.80665 \ ms^{-2}$	Gravitational constant
μ	0.02	Rolling coefficient
a	1.65 m	Length of FCHAMR
V_{ref}	24 V	Voltage reference
I_{aux}	3.65 A	Auxiliary current

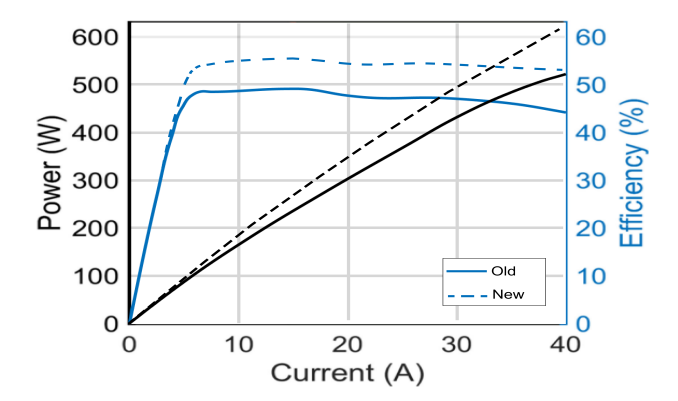


Figure 4: Horizon 500-W characteristic curves: Power and efficiency curve

2.2. FC modeling

This part introduces the hydrogen consumption model as well as the health model of the FC.

2.2.1. Hydrogen Consumption Model

The utilized FC is the PEMFC Horizon H-500. The characteristic curves of Horizon 500-W when new and after degradation have been generated and shown in Figure 4 (Kandidayeni et al., 2021).

The FC system is modeled by a semi-empirical equation (Yavuz et al., 2015), presented in Eq. 15, as:

$$V_{cell} = E_{nerst} - (V_{act} + V_{ohm} + V_{conc}) \tag{15}$$

where $V_{cell}(V)$ represents the FC cell voltage, $E_{nerst}(V)$ is the Nernst voltage, $V_{act}(V)$ is the activation voltage, $V_{ohm}(V)$ represents the ohmic voltage, and $V_{conc}(V)$ is the concentration voltage. The FC model is described by equations (16a-16d):

$$E_{nerst} = 1.229 - 0.85 \times 10^{-3} \times (T_{fc} - 298.15) + 4.3085 \times 10^{-5} \times T_{fc} \times (\ln P_{H_2} + 0.5 \ln P_{O_2}) \tag{16a}$$

$$V_{act} = \xi_1 + \xi_2 T_{fc} + \xi_3 T_{fc} \ln (CO_2) + \xi_4 T_{fc} \ln (i_{fc})$$
 (16b)

$$V_{ohm} = -i_{fc} \left(\mu_1 + \mu_2 T_{fc} + \mu_3 i_{fc} \right) \tag{16c}$$

Table 3Parameters for PEMFC Voltage Calculation

Parameter	Symbol	Value
Active Area	A_{cell}	50 cm ²
Number of Cells	N_{cell}	36
Fuel Utilization	U_{fuel}	80%
Air Utilization	U_{air}	40%
Operating Temperature	T_{fc}	65°C
Nernst Voltage Coefficient	ξ_1	1.229 V
Activation Voltage Coefficient	ξ_2	$-0.85 \times 10^{-3} \text{ V/K}$
Ohmic Resistance Coefficient	ξ_3	$4.3085 \times 10^{-5} \text{ V/K}$
Concentration Voltage Coefficient	ξ_4	1
Diffusion Mechanism Parameter	β	1.8
Flooding Phenomena Parameter	k	2

$$V_{conc} = \alpha \left(i_{fc} \right)^k \log \left(1 - \beta i_{fc} \right) \tag{16d}$$

Where T_{fc} (°C) is the FC temperature, $P_{H_2}(Pa)$ is the partial pressure of the hydrogen on the anode side, $P_{O_2}(Pa)$ represents the oxygen pressure on the cathode side, $C_{O_2}(g/L)$ is the oxygen concentration, $i_{fc}(A)$ represents the FC current, β represents a parameter related to diffusion mechanism (between 0.3 and 1.8), k denotes a dimensionless number related to the water flooding phenomena (between 1 and 4). $\xi_1, \xi_2, \xi_3, \xi_4, \mu_1, \mu_2, \mu_3, \alpha$ refer to the online parameters proposed by the model (Kandidayeni et al., 2021). Table 3 shows the parameters for PEMFC voltage calculation.

A model for calculating hydrogen consumption has been implemented, which is based on a 36-cell FC system. The amount of hydrogen consumed, denoted as $m_{H_2}(kg)$, can be determined using the methodology presented in (D. Zhou et al., 2017) with Eq. 17a and Eq. 17b:

$$m_{H_2} = \int_0^t \frac{P_{fc}}{\rho_{H_2} \eta_{fc}} dt$$
 (17a)

$$\eta_{fc} = \frac{P_{fc}}{P_{H_2}} \tag{17b}$$

In the above equations, ρ_{H_2} represents the chemical energy density of H_2 (measured in MJ/kg), $P_{fc}(W)$ is the net power output of the FC system, η_{fc} represents the efficiency of the FC system, and $P_{H_2}(W)$ denotes the theoretical power supplied by H_2 .

2.2.2. FC Health Model

The degradation of FC systems is a complex process influenced by various factors, spanning from electrochemical to mechanical aspects. Previous research (J. Wang et al., 2022) has highlighted the degradation sources, emphasizing catalyst layer, membrane layer, and gas diffusion layer degradation. When operating the FCHAMR, the FC is mostly susceptible to: startup-shutdown, low load, load change, high efficiency region load, and high load situations. This highlights the urgency for accurate and rapid predictive models to effectively manage FC health.

The FC voltage degradation can be calculated based on (H. Chen et al., 2015) as presented in Eq. 18:

$$V_t = N_{cycle}^1 v_1 + T_1 v_2 + N_{cycle}^2 v_3 + T_2 v_4 + T_3 v_5$$
(18)

Where N_{cycle}^1 represent the average startup-shutdown numbers per hour; T_1 represent the average low load time per hour; N_{cycle}^2 is the average load change cycles per hour, T_2 is the average high efficiency region load operation time per hour; T_3 is the high load operation time per hour. V_t stands for the average rate of voltage degradation per

Table 4
Voltage Degradation Rate Under Different Operating Conditions (Cell Level) (He et al., 2022)

Operating Conditions	Voltage Degradation Rate
Startup-shutdown	$v_1 = 13.79 \mu V/cycle$
Low load	$v_2 = 9.42 \mu V/h$
Load change	$v_3 = 0.04234 \mu V / kW$
High efficiency region load	$v_4 = 4.881 \mu V/h$
High power load	$v_5 = 11.67 \mu V/h$

hour while the vehicle is driving. v_1, v_2, v_3, v_4, v_5 represents the voltage degradation rate under the corresponding operating conditions, respectively (He et al., 2022). Table 4 shows the voltage degradation rate under different operating conditions (BenChikha et al., 2022).

To predict the lifetime of the FC, we employ a FC health model based on Long Short-Term Memory (LSTM) recurrent neural networks, as proposed in (H. Chen et al., 2015) and prior work of our laboratory (BenChikha et al., 2022). LSTM enables accurate lifetime prediction by learning non-linear degradation patterns, eliminating the need for in-depth understanding of FC degradation mechanisms and ensuring computational efficiency. The LSTM model, previously developed and tested in our laboratory, is trained using 90% of the voltage data and it demonstrates a high accuracy, with an overall Root Mean Square Error (RMSE) of approximately 0.0079 V. Figure 5 represents the resulting FC and LSTM fitted voltage signals and lifetime forecasting obtained from our previous work.

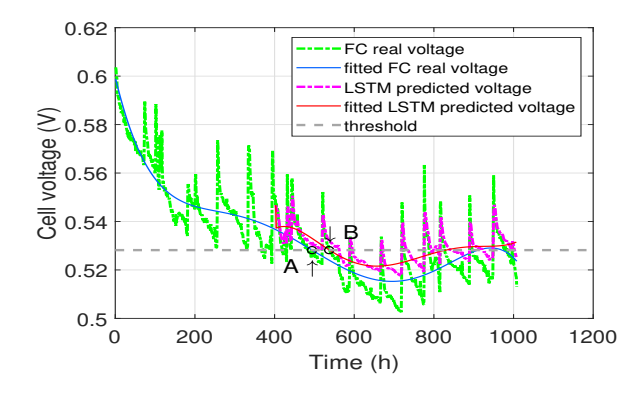


Figure 5: FC and LSTM fitted voltage signals and lifetime forecasting (previous work)

Furthermore, previous research has demonstrated that the shutdown process impacts the degradation rates (Zhang et al., 2018). The work in reference (Yu et al., 2012) revealed that utilizing an air starvation method during shutdown processes mitigates degradation, enhancing the FC's longevity. Therefore, the air starvation shutdown process was utilized for our experimental FC.

2.3. Battery model

In this study, a Lithium battery pack with a capacity of 40 Ah is used as the energy storage unit in the hybrid powertrain. Eq. 19 represents the open circuit voltage and Eq. 20 represents the internal resistance.

$$U_{ocv} = nU_1 \tag{19}$$

$$R_{bat} = nR_1 \tag{20}$$

Where $U_{ocv}(V)$ is the open circuit voltage of the battery pack, n is the number of cells in series, $U_1(V)$ is the open circuit voltage of the cell, $R_{bat}(\Omega)$ is the internal resistance of the battery pack and $R_1(\Omega)$ is the internal resistance of the single cell.

This paper uses the RINT model, which is shown in Eq. 21

$$U_{FCHAMR} = U_{ocv} - R_{bat}I_{bat} \tag{21}$$

Therefore, the expression of battery current is as follows in Eq. 22:

$$I_{bat} = \frac{U_{ocv} - \sqrt{U_{ocv}^2 - 4R_{bat}P_{bat}}}{2R_{bat}}$$

$$(22)$$

The SoC expression of battery is as follows in Eq. 23:

$$SoC(t+1) = SoC(t) - \frac{100I_{bat}(T)\Delta t}{3600Q_{bat}}$$
 (23)

Where SoC(t), $P_{bat}(W)$, $\Delta T(s)$, $Q_{bat}(Ah)$ are the battery state of charge, the battery power, the sampling interval and the nominal battery capacity, respectively.

2.4. Power system topology

The authors present in their work (Tran et al., 2020), a comprehensive analysis of power system topologies for FC electric vehicles. Among the various options, the active FC-battery topology comprises a unidirectional DC/DC converter for the FC system and a bidirectional DC/DC converter for the battery system. The choice of this topology is motivated by several factors (BenChikha et al., 2022). Firstly, this topology offers greater control over the FC and battery behaviors through the DC/DC converters, enabling efficient management of power flow. Secondly, it proves advantageous for recharging the battery. Lastly, it provides flexibility for future testing of alternative EMSs. However, it is essential to acknowledge certain drawbacks associated with this power topology, such as its higher cost and implementation complexity.

3. EMS with FC health control

This section introduces the design of an EMS that incorporates FC health-aware control. This strategy is composed of two steps: offline and online. A schematic diagram of the proposed EMS is shown in Figure 6.

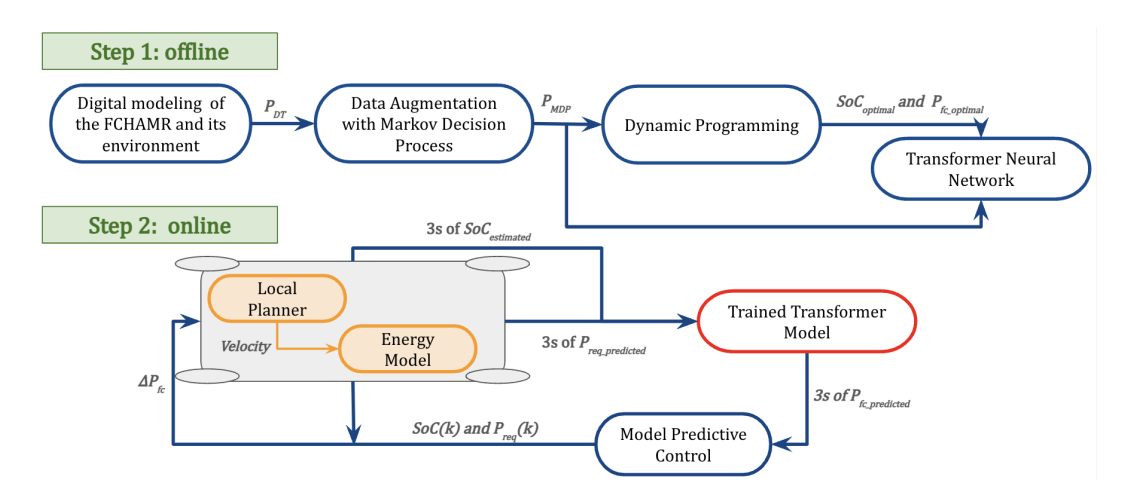


Figure 6: Proposed global methodology: Offline and Online modules

In this figure, P_{DT} represents the power profile obtained from digital modeling, while P_{MDP} is the augmented power profile derived from the MDP. The DP module outputs the optimal battery SoC, $SoC_{optimal}$, and the optimal FC power profile, $P_{fc_optimal}$. The estimated $SoC_{estimated}$ and predicted requested power $P_{req_predicted}$ are obtained from the local planner and energy model and represent the estimated SoC of the battery and the predicted requested power. $P_{fc_predicted}$ is the power of the FC as predicted by the Transformer model, and ΔP_{fc} represents the FC control

command calculated by the MPC. SoC(k) and $P_{req}(k)$ denote the battery SoC and requested power at instant k, which serve as the state variables for the MPC. For further clarification, Figure 7 provides a visual representation of the entire methodology's flowchart.

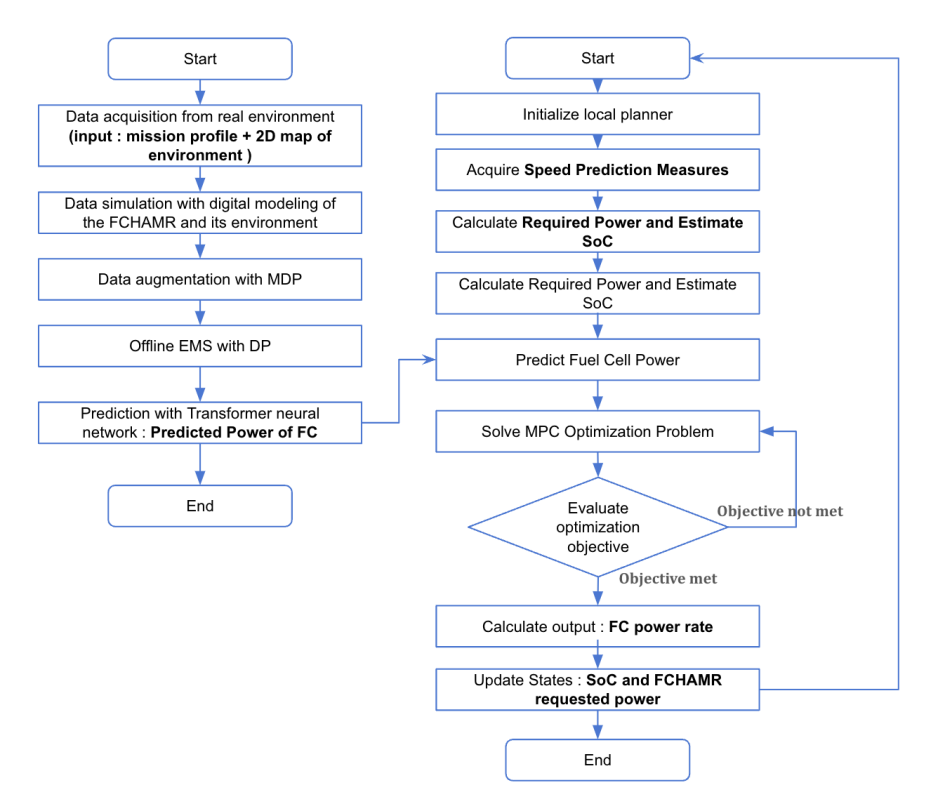


Figure 7: Proposed methodology flowchart

3.1. Offline energy management strategy

The offline module of the EMS incorporates several advanced techniques. A digital model of the FCHAMR and its environment is developed to rapidly acquire a comprehensive dataset describing the missions. This digital model allows to efficiently collect extensive and realistic data. To further enrich the dataset, a MDP is employed to generate requested power profiles based on input profiles derived from the digital simulations. The MDP outcomes serve as inputs for an offline EMS, which utilizes the DP algorithm. This algorithm optimizes the power allocation decision throughout the driving cycle. The optimized power allocation results obtained from the DP algorithm are subsequently utilized to train a Transformer neural network. This neural network model is trained to accurately predict the FC power output, given the requested power and the *SoC* of the battery. This combination of the DP-optimized power allocation and the Transformer neural network facilitates precise forecasting of the FC's power output.

3.1.1. Digital platform for data creation

Simulation is extensively used in robotics due to its potential advantages in cost savings and reduced testing times. One effective method for utilizing simulation is by creating a digital model of the FCHAMR and its surroundings using the Robot Operating System (ROS) (Mattila et al., 2022). This section details the generative digital modeling implementation, including specific algorithms and training procedures to enhance reproducibility and facilitate adoption. In this study, we model the physical properties of the FCHAMR, including its structure, obstacles, and the environment. Using a basic 2D map of the environment and a limited set of daily missions assigned to the FCHAMR, the digital reenacts these predefined missions while ingeniously generating supplementary tasks. Each driving mission is defined by key parameters such as the FCHAMR's localization, goal position, speed, wheel currents, and mass load. This approach eliminates the necessity of physical presence within the warehouse, enabling comprehensive data collection and insights without being on-site.

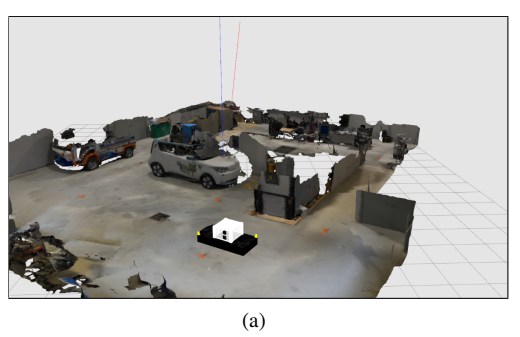




Figure 8: Gazebo environment: FCHAMR designed model, environment designed model: (a) lateral view (b) top view

To create an accurate digital space (environment and FCHAMR models), a comprehensive data acquisition process was undertaken. Real-time sensor data from the physical FCHAMR, including position, velocity, battery status, and environmental parameters, were collected. These data streams were integrated to establish a synchronized and up-to-date representation of the FCHAMR's operating conditions. Gazebo, a versatile 3D simulator, was used for environment modeling (Takaya et al., 2016). Gazebo generates sensor data, calculates physics, and creates specific robot models. This tool allows us to adjust a robot's dynamics realistically by modifying its inertial settings and accurately replicates specific environments, making it an ideal choice for developing the 3D digital model of the FCHAMR and its surroundings, including obstacles. Using Unified Robot Description Format (URDF) files, we defined the robot's kinematic and dynamic parameters, including mass, inertia, joint configurations, and sensor placements. Gazebo's physics engine, ODE (Open Dynamics Engine), was employed to simulate realistic interactions between the robot and its environment. We incorporated various plugins for sensor simulation, such as LiDAR and camera sensors, to generate accurate sensor data streams. Figures 8(a) and 8(b) illustrate the generated environment and the digital model of the FCHAMR. The digital implementation involves several key algorithms. The Simultaneous Localization and Mapping (SLAM) algorithm is used to generate a real-time occupancy grid map of the environment. The SLAM algorithm processes data from LiDAR and camera sensors to build and update the map while keeping track of the FCHAMR's location within it (Bailey & Durrant-Whyte, 2006). For path planning, a two-stage planning method is employed. The global planner utilizes algorithms such as A* or Dijkstra's to find the optimal geometric path to the next station while considering static obstacles. The local planner, Time Elastic Band (TEB) (Mohammadpour et al., 2024), then refines this path by generating feasible trajectories using translational velocity and rotational velocity (v, ω) as control signals to navigate dynamic obstacles and adhere to kinematic constraints (Malviya & Kala, 2021).

To ensure the digital space accurately mimics real-world conditions, the following training procedures were implemented. Real-world sensor data were augmented using noise models to simulate various environmental conditions and sensor inaccuracies, enhancing the robustness of the SLAM and path planning algorithms. The digital space conducted numerous missions, varying parameters such as maximum velocity, dynamic obstacles, and load conditions (e.g., adding three boxes, each weighing $18.5 \ Kg$). This variety in training scenarios ensures that the digital space can handle a wide range of operational conditions. A continuous feedback loop was established, where data from the digital simulations were compared with real-world mission outcomes. Discrepancies were analyzed to refine the algorithms and improve the fidelity of the digital space.

The generated map, depicted in Figure 9, represents the operating environment as an occupancy grid obtained using the SLAM algorithm. This figure illustrates one of the driving missions executed in the digital space. For the navigation of the FCHAMR, the global planner determines the geometric path to the next station, and the local planner (TEB) refines this path using control signals to follow the intended trajectory. The FCHAMR travels from the start station (point 1), pauses at way-point 2, and continues until reaching the finish point (point 3). This mission is repeated with varying parameters, and Figures 10(a) and 10(b) illustrate extracts of the driving cycle and the generated requested power profile, respectively.

3.1.2. Markov Decision Process for data augmentation

This paper proposes the use of a MDP-based approach to generate multiple mission profiles from a set of randomly collected mission profiles executed by the digital platform. The proposed approach works by analyzing the statistical

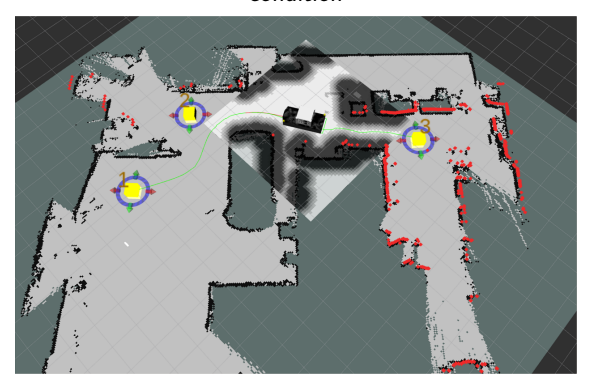


Figure 9: digital simulation example mission: scenario with 3 way-points (FCHAMR moves from 1 to 3) with a maximum linear velocity of $0.5 \, m/s^2$.

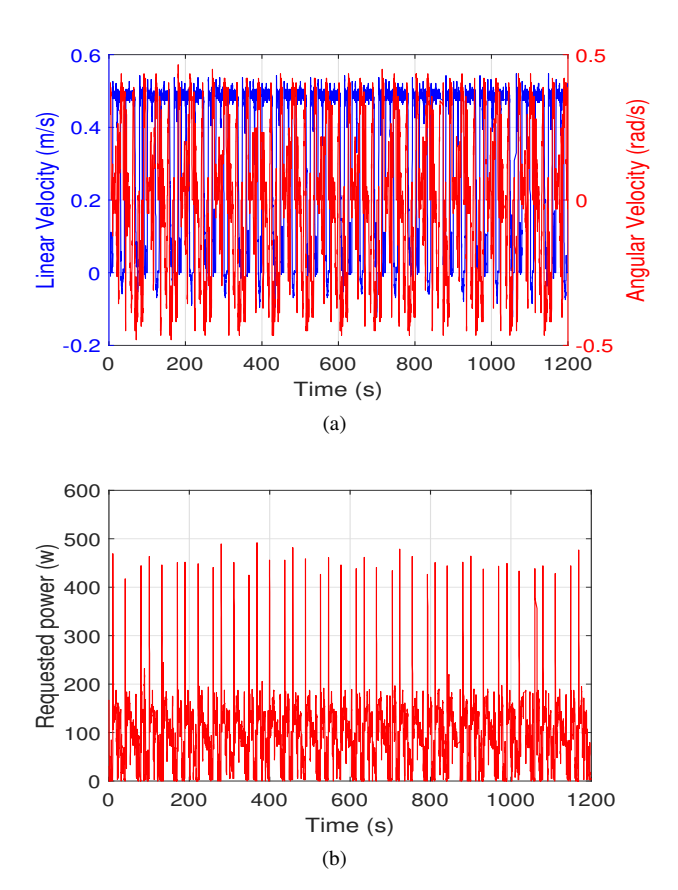


Figure 10: Digital space simulation data: (a) Extract of the driving cycle for 10 cycles of the mission. (b) Extract of the requested power profile for 10 cycles of the mission.

properties of the experimental mission profiles and using this information to construct a MDP. Then, this model generates a large number of synthetic requested power profiles that are statistically similar to the original data. The generated requested power profiles are used as inputs for the offline EMS. The use of multiple power profiles allows the energy management control to consider a variety of possibilities, making it more capable of handling a wider range of scenarios. In our health-aware energy management strategy for FCHAMRs, we utilize a MDP to augment the required power data. This approach ensures that we can generate diverse and realistic power demand profiles, enhancing the robustness of our predictive models and the overall energy management system (EMS). The MDP framework is defined

by a tuple (S, A, P, R, γ) , where S represents the states corresponding to power demands, A denotes the possible actions for transitioning between power states, P indicates state transition probabilities, R represents the rewards associated with state transitions, and γ is the discount factor. The states in our MDP correspond to different levels of required power (P_{req}) at each time step, reflecting the energy demand of the vehicle under various operational conditions. Formally, let $S = \{P_{req,1}, P_{req,2}, \dots, P_{req,N}\}$ be the set of possible power levels. The actions represent possible adjustments to the power demand, such as increasing or decreasing the required power, allowing the model to transition between different power states. Let $A = \{a_{increase}, a_{decrease}, a_{maintain}\}$ be the set of possible actions. The transition probabilities $P(P_{req,t+1} \mid P_{req,t}, a)$ define the likelihood of moving from one power state to another given a specific action. These probabilities are derived from historical power demand data and reflect the typical changes in power requirements over time. The reward function $R(P_{req}, a)$ is designed to encourage transitions that lead to realistic and varied power demand profiles, defined based on the similarity to observed data patterns and the diversity of generated profiles. To generate augmented power profiles, we utilize the Bellman equations to model the state transitions and optimize the generation process. The value function $V(P_{req})$ and Q-function $Q(P_{req}, a)$ are iteratively computed to determine the optimal action at each state to maximize the expected cumulative reward. The value function is given by

$$V(P_{req}) = \max_{a \in A} \left[R(P_{req}, a) + \gamma \sum_{P'_{req} \in S} P(P'_{req} \mid P_{req}, a) V(P'_{req}) \right], \tag{24}$$

and the Q-function is given by

$$Q(P_{req}, a) = R(P_{req}, a) + \gamma \sum_{P'_{req} \in S} P(P'_{req} \mid P_{req}, a) \max_{a' \in A} Q(P'_{req}, a').$$
(25)

Using the MDP framework, we generate new required power profiles by simulating the state transitions over a series of time steps. The process involves initializing from an initial power state $P_{req,0}$ based on observed data, selecting an action a_t at each time step t that maximizes the expected reward using the Q-function, transitioning to the next power state $P_{req,t+1}$ based on the selected action and the transition probabilities $P(P_{req,t+1} \mid P_{req,t}, a_t)$, and repeating the process for the desired number of time steps to generate a complete power profile. The data obtained with the digital space encompasses a total of 86400 seconds, equivalent to approximately 24 hours of constant operation of the FCHAMR. This dataset involves all the typical missions conducted by the FCHAMR throughout a day. To prepare for random events and add stochasticity to the repeated missions, the MDP generates data that extends to 432000 seconds, equating to 5 days of operation. By incorporating this extensive and varied dataset, we improve the predictive accuracy and robustness of the EMS, ensuring better performance and longevity of the FC under various operational conditions.

This article uses the Kullback-Leibler (KL) divergence to evaluate the similarity between the generated data set and the actual data, which is shown in Eq. 26:

$$D_{KL}(N||Q) = \sum_{i} P(i) \log \frac{N(i)}{Q(i)}$$
(26)

Where N represents the probability distribution of the actual data and Q represents the probability distribution of the generated data. The KL divergence $D_{KL}(N||Q)$ quantifies the variation between two probability distributions. The results revealed a minor difference between the two distributions, with the KL divergence being close to 0.032. Therefore, the additional driving cycles generated using the MDP accurately represent the selected data.

3.1.3. Dynamic Programming for offline optimal power allocation

Implementation of an offline energy management system which uses the long-term database will be discussed in this section based on (W. Zhou et al., 2018). The FCHAMR's work modes can be classified into four types: (1) Start Mode (SM), (2) Normal Work Mode (NWM), (3) Off Mode (OM), and (4) Battery Mode (BM). The unified state space equation of the DP model for FCHAMRs is established in Eq. 27a - 27b:

$$SoC(k+1) = SoC(K) - \frac{I(k)T_s}{3600Q\eta^{sgn(I(k))}}$$
 (27a)

$$P_F(k+1) = P_{fc_{out}}(k) \tag{27b}$$

$$M(k+1) = \psi(P_F, P_{fc_{out}}, k) \tag{27c}$$

Where the state variable is $x = [SoC, M, P_F]$, M represents the work mode, SoC represents the SoC of the battery and P_F denotes the power of the FC, the control variable is the power of the FC $P_{fc_{out}}$, I expresses the battery current, Q expresses the battery capacity, η expresses the coulombic efficiency of the battery, T_s expresses the time step, $\psi(P_F, P_{fc_{out}}, k)$, expresses the relationship between the work mode and the control variable. In addition, the change rate of the FC system power $\Delta P_{fc_{out}}$, can be calculated in Eq. 28:

$$\Delta P_{fc_{\text{out}}}(k) = P_{fc_{\text{out}}}(k) - P_F(k) \tag{28}$$

The parameters of the power system of a FCHAMR, including both state variables and control variables, must satisfy the following constraints in 29:

$$\begin{cases} P_{fc,min} < P_{fc} < P_{fc,max} \\ P_{bat,min} < P_{bat} < P_{bat,max} \\ P_{fc_{out},min} < P_{fc_{out}} < P_{fc_{out},max} \\ |\Delta P_{fc_{out}}| < \Delta P_{fc_{out},ratelimit} \\ SoC_{bat,min} < SoC_b < SoC_{bat,max} \end{cases}$$

$$(29)$$

Where P_{bat} is the battery power, P_{fc} is the FC power and $\Delta P_{fc_{out},rate}$ is the change rate of the FC power. The subscripts max and min refer to the maximum and minimum limits of each variable.

The optimization objective for the EMS of FCHAMRs includes the cost of frequent startup-shutdowns of the FC (L_{fc}) , the cost of work mode switching (L_M) , the cost of hydrogen consumption (L_{H_2}) , and the cost of electric energy consumption (L_{bat}) (2018).

Finally, the total cost is calculated by Eq. 30:

$$J = \Phi(x, N) + \sum_{k=0}^{N-1} L_{fc(k)} + L_M(k) + L_{H_2}(k) + L_{bat}(k)$$
(30)

Where $\Phi(x, N)$ is the cost of the terminal constraint and N represents the total number of calculation step. The DP algorithm for energy management consists of forward and backward calculations. During the forward calculation, for each requested power (P_{req}), a set of possible FC power outputs (P_{fc}) is generated, with each P_{fc} option associated with a specific cost. For each P_{fc} , the SoC of the battery is computed, and each SoC is assigned a cost, creating a tree of possibilities for P_{fc} and the corresponding SoC values. The mode filter of the FC is then applied, with each operational mode having an associated cost, further expanding the tree with additional possibilities based on the FC's mode. In the backward calculation, the algorithm evaluates the tree of possibilities and selects the combination of P_{fc} , SoC, and FC mode that results in the lowest total cost. By summing the costs associated with each combination, the optimal path is determined, ensuring a thorough exploration of all possible configurations and identifying the most cost-effective strategy for managing the energy distribution in the FCHAMR.

3.1.4. Transformer neural network for FC power prediction

The Transformer neural network is the neural network model used for this application (Vaswani et al., 2017) in order to predict the output power of the FC. The Transformer architecture has shown tremendous promise in forecasting problems (Reza et al., 2022) thanks to its effective handling of sequential input. The Transformer design is particularly suited for modelling time-series data because it can learn complicated correlations between inputs and outputs, and can handle long-term dependencies. The dataset from DP (the requested power, the battery's *SoC* and the FC power) is utilized as training data to train the Transformer model. The desired power and the battery's *SoC* are the inputs to the neural network, while the output is the FC power. Algorithm 1 represents the Transformer-Based Power Prediction Algorithm.

Algorithm 1 Transformer-Based Power Prediction Algorithm

```
1: Input: SoC and P<sub>rea</sub>
    \mathbf{X} = \{(SoC_t, P_{reqt})\}_{t=1}^T
 2: Output: Predicted power of the FC P_{fc}
 3: Initialization:
 4: Initialize model parameters: embedding dimension d, number of heads h, number of layers L, sequence length T
 5: Define embedding layer E: \mathbb{R}^2 \to \mathbb{R}^d
 6: Define positional encoding matrix PE \in \mathbb{R}^{T \times d}
 7: Define multi-head attention layers A_i for i \in \{1, ..., L\}
   Define feedforward network F_i for i \in \{1, ..., L\}
   Step 1: Encoding of Inputs
10: Apply embedding to inputs: \mathbf{H}_0 = E(\mathbf{X}) + PE {Add positional encodings}
11: Step 2: Attention Layers
12: for i = 1 to L do
     13:
            \mathbf{H}_i = A_i(\mathbf{H}_{i-1}) {Apply multi-head attention layer}
14: end for
15: Step 3: Feedforward Layers
16: for i = 1 to L do
            \mathbf{H}_i = F_i(\mathbf{H}_i) {Apply feedforward network}
    17:
18: end for
19: Step 4: Prediction of Power
20: Extract the final representation: \mathbf{H}_{final} = \mathbf{H}_{L}[:, -1, :] {Use the last time step's output}
21: Apply linear transformation to predict power: P_{fc} = \text{Linear}(\mathbf{H}_{final})
22: return P_{fc} = 0
```

The Transformer-based Power Prediction Algorithm is designed to accurately predict the power output of the FC using a Transformer neural network. The algorithm leverages the SoC and the requested power (P_{req}) as input variables to generate the predicted power output of the FC (P_{fc}) . The process involves several key steps, from initialization to the final prediction, as outlined below: First, the input sequence, which includes SoC and P_{req} over a time period T, is prepared. This sequence is denoted as $\mathbf{X} = \{(SoC_t, P_{reqt})\}_{t=1}^T$. The output of the algorithm is the predicted power of the FC, denoted as P_{fc} .

The algorithm begins with the initialization phase, where essential model parameters are set up. These parameters include the embedding dimension d, the number of attention heads h, the number of Transformer layers L, and the sequence length T. The embedding layer E is defined to convert the input sequence into a higher-dimensional space, facilitating better feature extraction and learning by the neural network. Additionally, a positional encoding matrix PE is defined to incorporate information about the position of each element in the sequence, which is crucial for the Transformer model to understand the order of the sequence. Next, the multi-head attention layers A_i for each of the L layers are defined. These attention layers allow the model to focus on different parts of the input sequence simultaneously, capturing various aspects of the data. Similarly, the feedforward networks F_i for each of the L layers are defined. These networks help in transforming the input data through multiple layers to extract complex features. In Step 1, the input sequence is encoded. The embedding layer E is applied to the inputs, and positional encodings PE are added, resulting in the initial hidden state H_0 . This step ensures that the model captures both the content and positional information of the input sequence. In Step 2, the encoded inputs pass through the multi-head attention layers. For each layer i from 1 to L, the hidden state from the previous layer \mathbf{H}_{i-1} is processed by the attention layer A_i . This step allows the model to attend to different parts of the input sequence, effectively capturing dependencies and relationships between the elements in the sequence. In Step 3, the output from the attention layers is further processed by the feedforward networks. For each layer i from 1 to L, the hidden state \mathbf{H}_i is transformed by the feedforward network F_i . This step helps in refining the features extracted by the attention layers, allowing the model to learn more complex representations of the input data. In Step 4, the final representation of the sequence is extracted. The output from the last Transformer layer \mathbf{H}_L is used, and only the representation corresponding to the last time step is extracted, denoted as $\mathbf{H}_{final} = \mathbf{H}_{L}[:, -1, :]$. This final representation encapsulates the information from the entire input sequence, focusing

Table 5
Evaluation metrics results

Metric	Value
RMSE	0.0081
MAPE	0.0921

on the most relevant features for the prediction task. A linear transformation is then applied to generate the predicted power output of the FC, Pfc. The linear transformation maps the high-dimensional representation to the desired output dimension, generating the predicted power value. The algorithm concludes by returning the predicted power of the FC, P_{fc} , which can be used for further analysis or as part of a larger energy management system. This Transformer-based approach ensures accurate and reliable power predictions, leveraging the advanced capabilities of attention mechanisms and deep neural networks.

To evaluate the accuracy of the predictions obtained from the different models, the following evaluation metrics (RMSE: Root Mean Square Error and MAPE: Mean Absolute Percentage Error) were used in Eq. 31 and Eq. 32:

$$RMSE = \sqrt{\frac{1}{n} \sum_{i=1}^{n} (y_i - \hat{y}_i)^2}$$
 (31)

$$MAPE = \frac{1}{n} \sum_{i=1}^{n} \left| \frac{y_i - \hat{y}_i}{\hat{y}_i} \right|$$
 (32)

Where \hat{y}_i is the predicted value and y_i is the actual value. Table 5 shows the values of the metrics.

According to an examination of the outcomes from the evaluation of the prediction model, the outcome is positive because it shows that the FC's power output can be predicted rather accurately by the prediction model. Thanks to the straightforward correlation in the data, the Transformer model can swiftly make predictions of the FC power in a matter of milliseconds.

3.2. Online energy management strategy loop based on Model Predictive Control

The proposed methodology employs the local planner to predict the FCHAMR's velocity by considering factors such as static and dynamic obstacles, and the desired path. This prediction is then used in the energy model to calculate the required power for achieving the desired velocity. Subsequently, this predicted power requirement is used as input for the trained Transformer model to forecast the FC power.

In this work, a predictive model based on a non-linear time-invariant state-space representation of the FCHAMR is utilized (Martínez et al., 2013b). It includes the battery's SoC, the FC's hydrogen consumption rate, and the system's power demand. MPC solves an optimization problem at each time step, aiming to minimize a cost function that considers the deviation from the reference signal obtained from offline energy management. To account for system dynamics, MPC operates in a receding horizon manner, optimizing over a finite time horizon. Control actions are applied at each step, and the optimization problem is solved anew with updated measurements for subsequent time steps.

This study adopts a model focusing on non-linear discrete-time control, where the state space functions and system variables are defined as follows:

$$x_{k+1} = A(k)x(k) + B_u(k)u(k) + B_v(k)v(k)$$
(33)

$$y(k) = Cx(k) + Du(k) \tag{34}$$

In the predictive control strategy, the length of the control horizon is set to be the same as its prediction horizon H_p , with a sampling period $\Delta T = 20$ ms. Here, x(k) is the state variable $x(k) = [SoC(k), P_{fc}(k-1)]^T$, u(k) is the control variable $u(k) = \Delta P_{fc}(k)$, v(k) is the disturbance signal obtained from the offline EMS $v(k) = P_{req}(k)$, and

y(k) is the output variable $y(k) = [SoC(k), P_{fc}(k)]^T$. Meanwhile, the power balance relationship can be expressed in the discrete form as follows:

$$P_{reg}(k) = P_{hat}(k) + P_{fc}(k) \tag{35}$$

Additionally, the battery SoC dynamics are modeled by first-order differential equations represented as:

$$SoC(k+1) = SoC(k) - \frac{100P_{bal}(k)\Delta T}{3600Q_{bal}U_{FCHAMR}(k)}$$
(36)

Where U_{FCHAMR} denotes the FCHAMR voltage. The system matrices can be determined as follows:

$$A(k) = \begin{bmatrix} 1 & \frac{100\Delta T}{3600Q_{bal}U_{FCHAMR}(k)} \\ 0 & 1 \end{bmatrix}$$
 (37a)

$$B_{u}(k) = \begin{bmatrix} \frac{100\Delta T}{3600Q_{bal}U_{FCHAMR}(k)} \\ 1 \end{bmatrix}$$
 (37b)

$$B_{\nu}(k) = \begin{bmatrix} -\frac{100\Delta T}{3600Q_{bat}U_{FCHAMR}(k)} \\ 0 \end{bmatrix}$$
 (37c)

$$C = \begin{bmatrix} 1 & 0 \\ 0 & 1 \end{bmatrix} \tag{37d}$$

$$D = \begin{bmatrix} 0 & 1 \end{bmatrix} \tag{37e}$$

The objective is to track the reference power of the FC. This can be accomplished by defining an objective function J as follows:

$$J_{i} = \sum_{m=i}^{i+H_{p}} \left(P_{fc,ref}(m) - P_{fc}(m) \right)^{2}$$
(38)

where $P_{fc,ref}$ represents the power of the FC from the reference signal.

To ensure the proper operation of the power sources, constraints should be established before making control decisions. The constraints on the FC system are expressed as:

$$\begin{cases} 0 \le P_{fc}(k+i) \le \overline{P_{fc}} \\ -\overline{\Delta P_{fc}} \le \Delta P_{fc}(k+i-1) \le \overline{\Delta P_{fc}} \end{cases}$$
(39)

where $\overline{P_{fc}} = 500 \text{ W}$ and $\overline{\Delta P_{fc}} = 1 \text{ W/s}$.

The power allocation decision in the *i*-th receding horizon is expressed mathematically as:

$$\min_{\Delta P_{fc}(k), k = i, \dots, i + H_p - 1} J \tag{40}$$

In this solution, for the optimal control sequence $\left[P_{fc}^*(i), \dots, \Delta P_{fc}^*\left(i + H_p - 1\right)\right]$, only the initial element $\Delta P_{fc}(i)$ is applied to the hybrid powertrain model, with the remaining elements discarded. At the next time step, the system state is updated, and optimization is re-executed to determine the subsequent control action (He et al., 2022).

4. Results and discussion

In the following section, the benchmarking techniques utilized for evaluation will be outlined, and the obtained results will be subsequently discussed.

DP provides the optimal solution and is thus the gold standard for benchmarking. Other energy management algorithms, particularly online algorithms, are compared with results from DP. The DP Benchmark is the one utilized in 3-1-3 with the cost function indicated in Eq.(30) and constraints shown in Eq.(29). DP is highly effective in delivering the most energy-efficient and health-preserving outcomes possible under offline conditions. However, DP's computational intensity and sensitivity to predefined operational cycles make it impractical for real-time application in dynamic settings, where energy demand and system conditions fluctuate frequently. For this reason, DP is used here as an offline benchmark.

Moreover, a multi-objective MPC-based strategy is adopted for comparison, as shown in (2022). The benchmark MPC provides near-optimal solutions by solving a constrained optimization problem at each step, making it more adaptable to real-time conditions compared to DP. However, due to the complexity of the MPC's cost function, execution times can be relatively long, which may limit its effectiveness in highly dynamic applications where fast, responsive adjustments are required. Nevertheless, comparing the proposed method with both DP and the benchmark MPC offers valuable insights into EMS performance, balancing optimality with practical real-time feasibility.

The performance of the developed EMS for the studied FCHAMR is assessed through both simulation and experimental tests conducted in the lab of the Hydrogen Research Institute (IRH) at the University of Quebec in Trois-Rivières. The experimental setup includes a comprehensive array of sensors for current, voltage, speed, and position measurements, all interfaced with a real-time embedded control system running the developed EMS. Data acquisition is handled by a National Instruments (NI) system, ensuring precise logging of sensor data and system states throughout the experiments. The experimental environment is a dedicated section of the lab, equipped with multiple workstations to simulate different operational stations for the FCHAMR. The driving cycle within the lab involves the FCHAMR navigating between these stations, simulating typical transport tasks. During this cycle, the EMS dynamically manages the power distribution between the FC and the battery based on real-time data inputs. Sensor data and control signals are continuously recorded, with the data acquisition system capturing all relevant parameters for detailed post-experimental analysis.

In parallel to these experimental tests, the EMS is also validated through MATLAB simulations. The same driving cycle and system parameters are employed in the simulations to ensure consistency and allow for a thorough comparison between experimental and simulated results. The MATLAB environment models the FC, battery, and FCHAMR dynamics, providing a comprehensive validation of the EMS. Post-processing and analysis of the collected data from both the experimental setup and MATLAB simulations are performed to evaluate key performance metrics, including energy efficiency, FC hydrogen consumption, battery SoC variation, and overall system reliability. This rigorous experimental setup and procedure ensure that the developed EMS is extensively tested under controlled conditions, yielding valuable insights into its performance and potential improvements. The detailed approach validates the EMS's robustness and efficiency in managing the power demands of the FCHAMR.

Figure 11 represents the mission executed by the FCHAMR for testing the algorithms. The FCHAMR, moving at a top speed of 0.8 m/s, efficiently navigates from station 1 to station 4 and stops at waypoints 2 and 3 while carrying three loads. Throughout this process, the vehicle encounters occasional interruptions caused by both moving and stationary obstacles. While the FCHAMR is moving, the local planner affects velocity predictions. Simultaneously, the required power is calculated through the energy model and input into the Transformer model during each prediction step. This model forecasts FC power, which is then supplied to the MPC for dynamic reference in control. Figure 12(a) and Figure 12(b) illustrate the FCHAMR's driving cycle across multiple iterations throughout the entire mission as well as the requested power profile.

Figure 13 demonstrates the tracking of the FC's reference power by the proposed MPC technique. The estimated power production follows the reference power with minimal deviation. To maintain the FC at the optimal power level while adhering to constraints, the MPC algorithm adeptly adjusts control inputs in real time. This dynamic adjustment is pivotal for the efficient operation of the FC system.

Three control strategies are evaluated on the same requested power based on hydrogen consumption and startup-shutdown frequency. Figure 14 denotes a comparison of the *SoC* trajectory of the battery. All strategies have the same initial *SoC* and final *SoC* which allows us to evaluate the performance of the FC at each method. Two similar SoC profiles are obtained in the proposed MPC strategy (Proposed method) and the Benchmark MPC strategy due to the fact

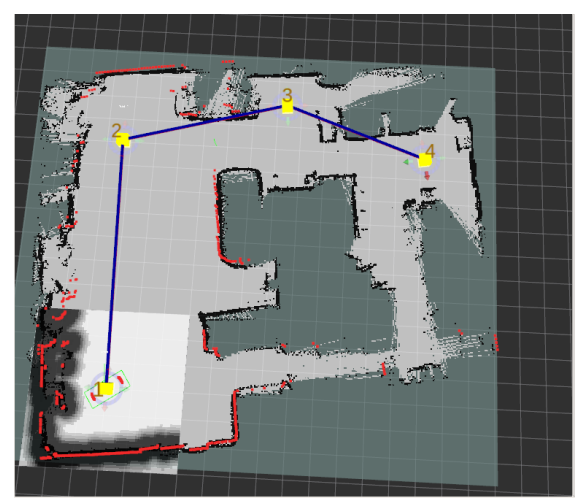


Figure 11: Testing scenario: Testing Mission: start station 1, waypoints 2 and 3, final station 4 (The blue lines represent the links between the stations and the waypoints).

Table 6
Comparison of number of startup-shutdown cycles for 600s

Control strategies	Number of startup-shutdown cycles
DP	1
Proposed method	3
Benchmark-MPC	10

that both of them rely on the same cost function. This indicates that both strategies aim to optimize the battery's state of charge in a similar manner. However, the Benchmark MPC still uses the battery more than the proposed method.

The results of the offline DP implementation, in Figure 15(a), have shown that it has achieved similar results compared to the proposed method in Figure 15(b). Certainly, the interval between 10 to 30 seconds notably highlights the smoother power profile of DP in contrast to the proposed strategy. This disparity can be attributed to the offline nature of DP, allowing it to optimize power allocation comprehensively beforehand, ensuring a more consistent and stable power output. In contrast, our online method might encounter slight fluctuations due to real-time adjustments during the actual operation, leading to a marginally less smooth power profile in certain scenarios. Although the proposed strategy might experience slight deviations, especially in response to abrupt changes, it still holds the potential to yield results comparable to the ideal standards in real-time implementations.

Figure 15(c) illustrates the performance of the MPC-based benchmarking technique for managing the energy of FCHAMRs. Compared to Figure 15(b), Figure 15(c) illustrates that the Benchmark MPC method displays more noticeable startup-shutdown patterns all along the driving cycle and inaccurate fluctuations particularly within the 140 to 160-second window. Consequently, the inaccuracies stem from the method's calculation approach, impacting its ability to swiftly align with the power demands issued by the FCHAMR. Table 6 provides a detailed breakdown of startup-shutdown occurrences for each methodology for the total driving cycle. The DP approach demonstrates good stability with just one cycle. The proposed method strategy shows a slightly higher count of three cycles, while the Benchmark-MPC strategy exhibits more variability with ten cycles. This comparison highlights the differences in control decisions and precision among the evaluated strategies.

Figure 16 represents the total hydrogen consumption for each method. The DP method exhibits a relatively low consumption rate of 12.97 g, indicating its efficient utilization of hydrogen during the 600-second operation. On the other hand, the proposed method slightly increases the consumption to 15.83 g, suggesting a marginally higher demand, potentially due to its real-time adaptive nature. In contrast, the Benchmark MPC displays a higher consumption rate at 20.13 g, emphasizing its limitations in optimizing hydrogen usage.

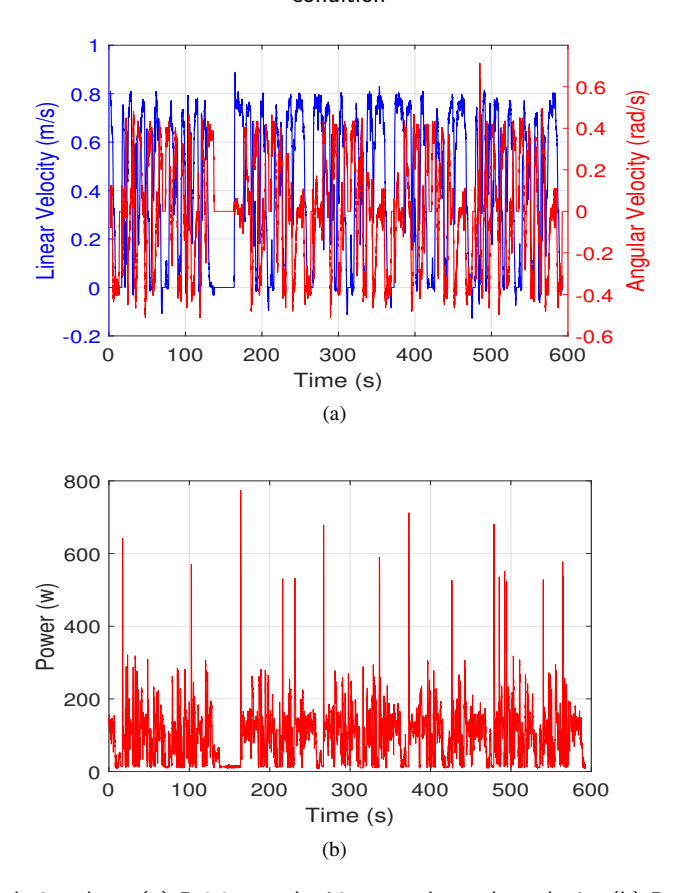


Figure 12: Digital simulation data: (a) Driving cycle: Linear and angular velocity (b) Requested power profile.

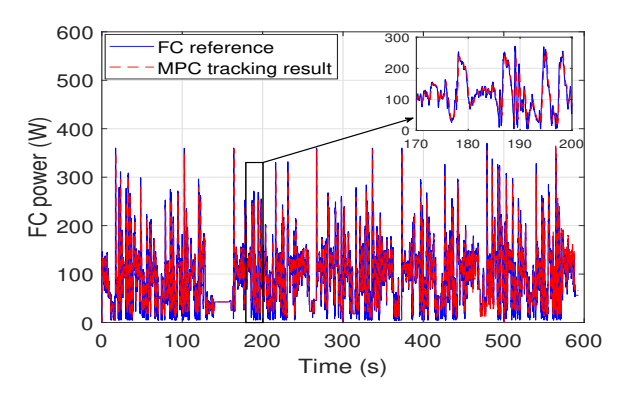


Figure 13: MPC Tracking Results compared with the reference signal

Figure 17 presents the estimated FC lifetime (in hours) for the three control strategies after repeating the driving cycle for 10,000 iterations. The lifetime is predicted using the method in 2.2.2. Among them, the DP control strategy exhibits a lifetime value of 2760 hours, followed closely by the proposed method strategy with 2697 hours and the Benchmark-MPC strategy with 2412 hours. The findings indicate that the proposed method approach enhances the FC lifespan compared to the Benchmark-MPC, extending it by 285 hours (9.5%). A relatively short timeline of 63 hours (2.1%) separates the lifetime optimization gap from the DP strategy. These outcomes underscore the proposed strategy's effectiveness in prolonging the FC's operational life. Figure 16 and Figure 17 reveal a strategic compromise to balance the degradation incurred by frequent startup-shutdown cycles with the overall hydrogen consumption in the

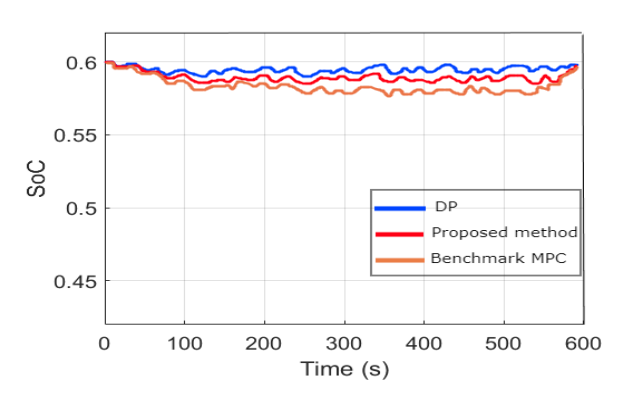


Figure 14: Comparison of the SoC trajectory of battery

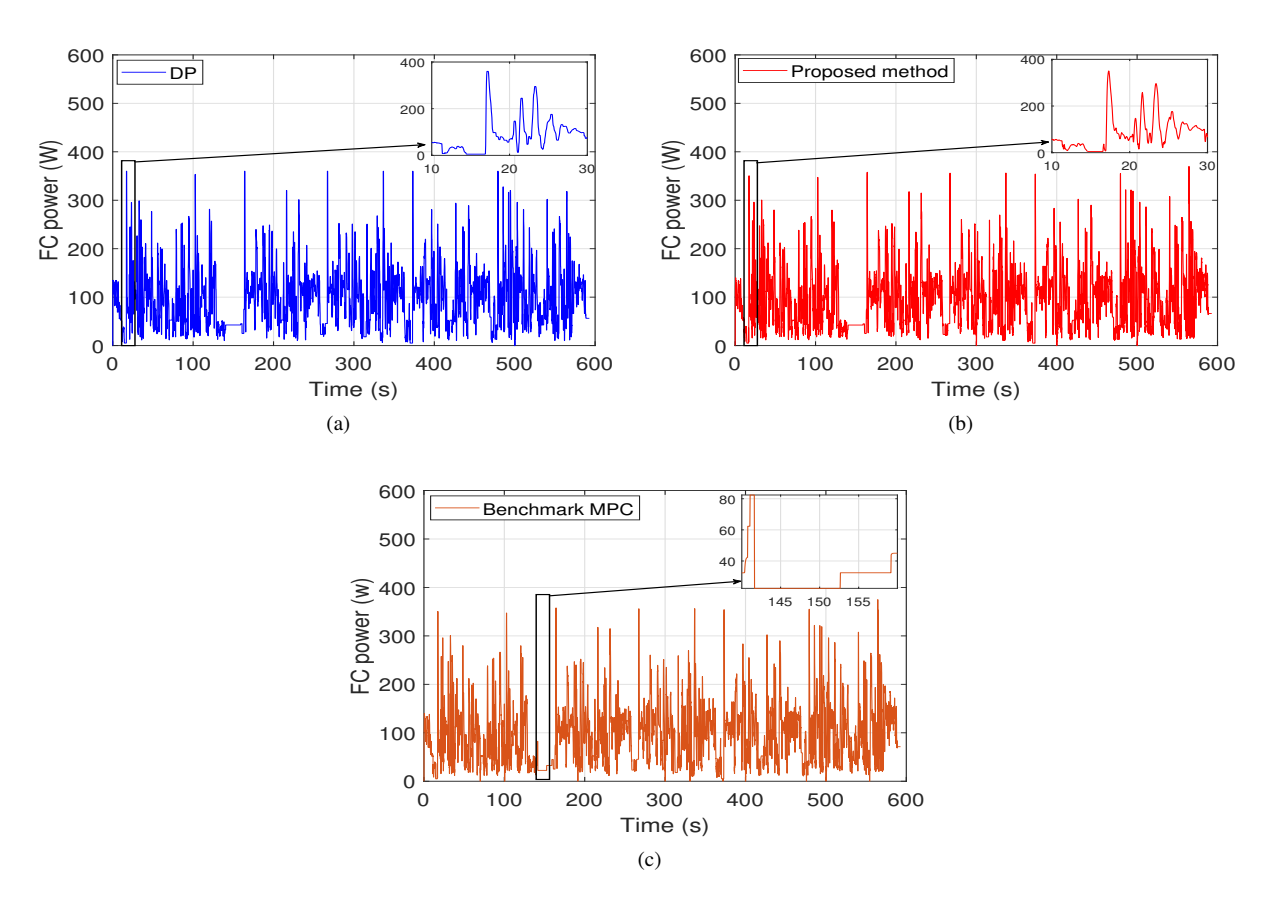


Figure 15: The results of FC power output for the three control strategies: (a) DP, (b) proposed method, (c) Benchmark-MPC

proposed methodology. This equilibrium is important in real-world applications, where the longevity of the FC must be safeguarded without compromising efficiency or power output.

The average running time for each step for the three real-time energy management techniques is shown in Table 7. The Benchmark MPC method requires the most computation time (46.5 ms), highlighting its computational complexity. The running time per step of the proposed strategy is 20 ms, which is equal to the period needed for the local planner to update its value. The ability to deliver updates within the stringent time constraints of the local planner

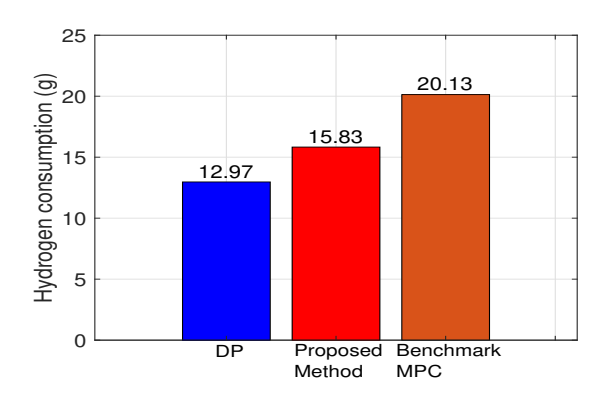


Figure 16: Hydrogen consumption results

Table 7Comparison of online running time

Control strategies	Average running time per step (ms)
Proposed method	20
Benchmark MPC	46.5

(20 ms) demonstrates the light computational complexity of our methodology and ensures its integration into real-time applications. This efficiency is paramount in dynamic environments, where rapid decision-making is essential. Therefore, the proposed methodology optimizes FC performance with fast speed, setting it apart as a robust and practical solution compared to the online benchmarking technique.

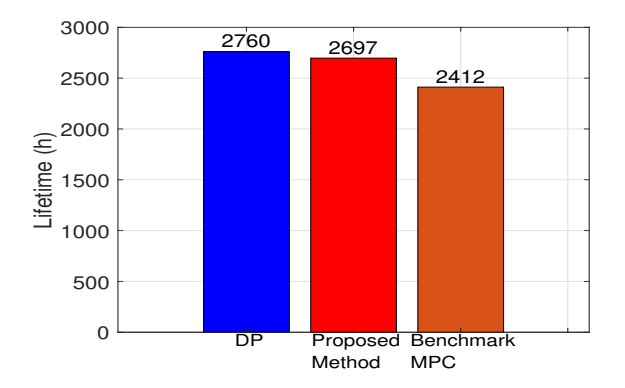


Figure 17: Estimated FC lifetimes

To validate the effectiveness of the proposed EMS, paired t-tests (Rietveld & van Hout, 2017) were conducted to compare the performance metrics of the proposed method against those of both the DP and benchmark MPC strategies. Key performance metrics, including hydrogen consumption, startup-shutdown cycles, and remaining useful life, were measured across multiple experimental runs to ensure reliability. Each metric was evaluated for normality with the Shapiro-Wilk test before performing paired t-tests at a 0.05 significance level. The results showed that the proposed EMS achieved a statistically significant reduction in hydrogen consumption compared to the Benchmark MPC, with a mean difference of 4.3 g (p < 0.01 < 0.05), and a slightly higher but comparable consumption to the offline DP method, with a mean difference of 2.86 g (p < 0.05). Regarding startup-shutdown cycles, the proposed method averaged 3 cycles, demonstrating a reduction compared to the 10 cycles observed in Benchmark MPC (p < 0.01 < 0.05), while showing only a slight increase from the single cycle in the DP (mean difference of 2 cycles, p < 0.05). For remaining useful life, the proposed EMS achieved an increase of 285 hours over the Benchmark MPC (p < 0.01 < 0.05),

with a more marginal difference of 63 hours compared to DP (p < 0.05). These statistical findings underscore that the proposed EMS not only aligns closely with the offline-optimal DP method but also significantly outperforms the Benchmark MPC in fuel efficiency, startup frequency reduction, and operational lifespan extension.

In addition to the simulation-based investigations, experimental tests were conducted using the same driving cycle to validate the proposed approach. Figure 18 presents a comprehensive comparison between the simulation results and the actual experimental data. The experimental findings align with the simulation results, displaying similar trends with minor discrepancies observed. Through the highlighted rectangles, a subtle delay of roughly 3 seconds (monitored within the experiment) has surfaced between observed results and their simulated counterparts. While seemingly minor, this temporal gap offers insight into the complex interplay between reality and digital modeling, influenced by factors like data processing and computational intricacies. However, the trend of the curves demonstrates that the proposed method is still capable of tracking the results. The consistency between the simulation and experimental outcomes highlights the potential of the approach to provide reliable and efficient energy management for FCHAMR, bridging the gap between theoretical modeling and real-world application.

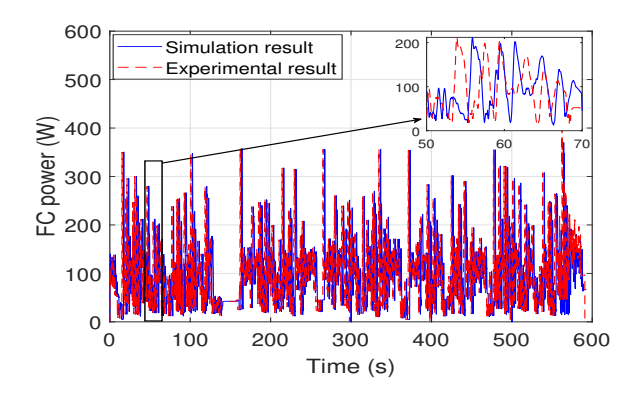


Figure 18: Experimental results vs simulation results

Additionally, to ensure the robustness of our method, we evaluated its performance under varying operational conditions. Table 8 presents the comparison metrics for standard, high load, low load, high velocity, low velocity, and varied acceleration conditions on the mission shown in 11. These results further demonstrate the effectiveness of our proposed method in optimizing energy management for FCHAMRs.

To further illustrate the performance of our proposed method, we conducted additional simulations varying the mission duration. Table 9 compares the hydrogen consumption, startup-shutdown cycles, and remaining useful life under different mission times for the three control strategies. The table highlights the superior performance of our proposed method in terms of hydrogen consumption, startup-shutdown cycles, and remaining useful life compared to the benchmark MPC.

The analysis of performance metrics under varying operational conditions, as seen in Table 8, provides a comprehensive evaluation of the proposed method's robustness and adaptability. In standard conditions, the proposed method demonstrates a balanced performance with hydrogen consumption slightly higher than DP but significantly lower than the Benchmark MPC. This indicates that while our method is not as optimal as the offline DP, it still offers substantial improvements over traditional online methods.

Under high load conditions, the proposed method maintains its efficiency, showcasing its ability to handle increased power demands with relatively modest increases in hydrogen consumption and startup-shutdown cycles compared to DP. The remaining useful life of the FC under high load conditions further underscores the method's effectiveness in managing degradation, with a minimal reduction in lifespan. In low load conditions, the proposed method performs exceptionally well, with hydrogen consumption and startup-shutdown cycles only slightly higher than DP and significantly lower than the Benchmark MPC. This highlights the method's capability to optimize energy usage and reduce wear and tear on the FC during less demanding operations. When subjected to high velocity, the proposed method again demonstrates its adaptability by effectively managing higher power requirements and maintaining a reasonable hydrogen consumption rate. The startup-shutdown cycles are slightly higher than DP, but the remaining useful life indicates that the method effectively mitigates the impact of increased operational speed on FC degradation.

Table 8Performance Metrics Comparison Under Varying Operational Conditions

Condition	Metric	DP	Proposed	Benchmark MPC	
Standard	H ₂ Consumption (g)	12.97	15.83	20.13	
	Startup-shutdown Cycles	1	3	10	
- Courrage C	Remaining Useful Life (h)	2999.9799	2999.9695	2999.9470	
	H ₂ Consumption (g)	14.81	17.57	21.00	
High Load	Startup-shutdown Cycles	2	4	11	
	Remaining Useful Life (h)	2999.9798	2999.9693	2999.9468	
Low Load	H ₂ Consumption (g)	11.50	13.44	19.00	
	Startup-shutdown Cycles	0	2	9	
	Remaining Useful Life (h)	2999.9799	2999.9697	2999.9472	
High Velocity	H ₂ Consumption (g)	14.53	18.11	22.24	
	Startup-shutdown Cycles	2	5	12	
	Remaining Useful Life (h)	2999.9798	2999.9692	2999.9465	
Low Velocity	H ₂ Consumption (g)	12.01	15.10	19.78	
	Startup-shutdown Cycles	1	3	10	
	Remaining Useful Life (h)	2999.9799	2999.9694	2999.9471	
Varied Acceleration	H ₂ Consumption (g)	13.02	16.22	20.81	
	Startup-shutdown Cycles	2	4	11	
	Remaining Useful Life (h)	2999.9798	2999.9693	2999.9468	

Table 9
Performance Metrics Comparison Under Varying Mission Times

Mission Time	Metric	DP	Proposed	Benchmark MPC
H ₂ Consumption (g)		12.97	15.83	20.13
600 seconds Startup-shutdown Cycles		1	3	10
Remaining Useful Life (h)		2999.97	2999.96	2999.94
4 hours	H ₂ Consumption (g)	51.88	63.32	80.52
	Startup-shutdown Cycles	4	12	40
	Remaining Useful Life (h)	2999.42	2999.26	2998.58
24 hours	H ₂ Consumption (g)	311.28	379.92	482.88
	Startup-shutdown Cycles	24	72	240
	Remaining Useful Life (h)	2996.52	2995.60	2991.48
5 days	H ₂ Consumption (g)	1556.40	1898.80	2414.40
	Startup-shutdown Cycles	120	360	1200
	Remaining Useful Life (h)	2982.60	2978.04	2957.40

Conversely, under low velocity conditions, the proposed method closely mirrors the performance of DP, with only marginal differences in hydrogen consumption and startup-shutdown cycles. This consistency in performance across different speeds showcases the method's robustness in varying operational scenarios. In varied acceleration conditions, the proposed method maintains a balanced performance, demonstrating its ability to handle dynamic changes in power demands effectively. The hydrogen consumption and startup-shutdown cycles are well-managed, ensuring minimal impact on the FC's remaining useful life.

Additionally, the performance metrics under varying mission times, as illustrated in Table 9, further emphasize the robustness and adaptability of the proposed method. As mission time increases, the advantages of the proposed method become more pronounced. For shorter missions, such as 600 seconds, the proposed method shows a slight advantage in hydrogen consumption and startup-shutdown cycles compared to the Benchmark MPC, maintaining efficiency in short-duration tasks common in industrial environments. As the mission extends to 4 hours, the benefits

become more evident. The hydrogen consumption remains significantly lower than the Benchmark MPC, highlighting superior fuel efficiency. The reduced startup-shutdown cycles suggest better management of power transitions, crucial for maintaining FC health and longevity. The longer remaining useful life of the FC under our method validates the effectiveness of our energy management strategy. When the mission time is increased to 24 hours, the proposed method continues to demonstrate its advantages with markedly lower hydrogen consumption and controlled startup-shutdown cycles, ensuring minimal wear and tear on the FC. This efficiency is crucial for sustaining long-term operations, with our method showing a significantly longer remaining useful life compared to the Benchmark MPC. For extended missions, such as 5 days, the strengths of our method are even more pronounced. The significant reduction in hydrogen consumption and controlled startup-shutdown cycles highlight exceptional fuel efficiency and effective power management over prolonged periods. The substantial increase in the remaining useful life of the FC demonstrates our method's superior capability in preserving FC health and ensuring sustained operational efficiency.

5. Conclusion

In this paper, an online energy management strategy for a FCHAMR with FC health awareness control is proposed to optimize hydrogen consumption and the startup-shutdown frequency of the FC, based on a two-module framework. The following are some of the paper's significant contributions:

- Developing methods to generate and utilize detailed and comprehensive datasets that reflect the specific operational conditions of FCHAMRs. This is facilitated through the introduction of a generative digital modeling-MDP approach, enabling rapid generation of diverse requested power profiles for FCHAMRs and eliminating the need for extensive manual data collection in industrial settings.
- Balancing hydrogen consumption and FC degradation induced by recurrent startup-shutdown cycles, ensuring the longevity of the FC as well as the energy efficiency of the system in dynamic industrial environments. This contribution is introduced through the first step of the EMS, including the optimal offline power distribution with Dynamic Programming (DP).
- Handling the high level of adaptability required for FCHAMRs by using an online Model Predictive Control
 (MPC) based EMS with input from Transformer neural network power prediction, adaptive to real-time
 adjustments. This step allows the EMS to effectively respond to instantaneous energy demand fluctuations in
 dynamic and unpredictable environments.

Through analysis and real-time energy management, the proposed method has demonstrated significant outcomes. Indeed, the developed approach has extended the FC's estimated lifetime while optimizing hydrogen consumption. The results underscore the effectiveness of our EMS, providing an optimal solution for the complex challenges faced in FCHAMR applications.

However, the study also reveals several limitations and challenges that need to be addressed to further enhance the EMS's performance. Theoretical limitations include reliance on predefined models, which may not fully capture the FC's dynamic and complex behavior under all conditions. Optimization-based methods used in the EMS are subject to both model and aleatory uncertainties, which can affect the reliability and robustness of the EMS in dynamic environments. These factors impact optimization consistency, challenging reliable EMS performance under variable conditions Practical limitations are evident in the experimental validation phase, where various real-world conditions and disturbances must be considered to evaluate the EMS's performance comprehensively. Ensuring robustness and reliability in such diverse and unpredictable environments is a significant challenge. Addressing these challenges requires innovative approaches to streamline data processing and integration while maintaining high computational efficiency.

Future research will focus on several key areas to address these limitations. First, it should focus on utilizing more sophisticated and flexible models that can adapt to a wider range of scenarios, addressing these uncertainties to improve robustness. Second, Developing methods for continuously monitoring the FC state through online parameter identification is crucial. This approach will create a more adaptive EMS, dynamically adjusting based on the FC's specific needs to ensure optimal operation under various conditions. Including the load mass in this process will optimize real-time power distribution. Predicting the FC's future health state will enhance the EMS by forecasting degradation trends, anticipating maintenance needs, and extending operational life. Expanding the current digital space

into a comprehensive digital twin containing all FCHAMR resources and operational data would significantly improve EMS functionality. A fully integrated digital twin would enable real-time monitoring, analysis, and optimization by mirroring physical system dynamics and environmental conditions, allowing for precise predictive adjustments in energy management. Leveraging data from the digital twin will allow for proactive optimization of energy management strategies, adapting to changing conditions to maximize efficiency and extend FC life. Finally, experimental validation of the strategy after integrating all the modules is crucial to ensure effective operation in real-world conditions. Addressing these areas will provide a more robust and efficient EMS for FC hybrid autonomous mobile robots, tackling current limitations and future challenges. This research represents a significant step towards enhancing the energy efficiency and operational longevity of autonomous mobile robots in industrial environments.

Nomenclature

General		F_{aero}	Aerodynamic force (N)
α	Angle of inclination (radians)		Gravitational constant $(9.80665 m/s^2)$
β	Diffusion Mechanism Parameter (dimensionless)	I	Inertia of the FCHAMR $(kg \cdot m^2)$
Δt	Sampling interval (s)	I_{aux}	Current withdrawn by the auxiliary components
η_{cont}	DC/AC converter efficiency (dimensionless)		(A)
η_{fc}	Efficiency of the FC system (dimensionless)	I_{bat}	Battery current (A)
η_{mot}	Motor's efficiency (dimensionless)	i_{fc}	FC current (A)
η_{tr}	Transmission system efficiency (dimensionless)	k	Flooding Phenomena Parameter (dimensionless)
μ	Coefficient of rolling friction (dimensionless)	m	Total mass of the FCHAMR (kg)
ω	Angular velocity of the FCHAMR's center of	m_{H_2}	Mass of hydrogen consumed (kg)
	mass (rad/s)	$N_{cell}^{^{2}}$	Number of cells (dimensionless)
ω^L	Rotational velocity of the left wheels (rad/s)	$N_{cell}^{2} \ N_{cycle}^{1}$	Average startup-shutdown numbers per hour (di-
ω^R	Rotational velocity of the right wheels (rad/s)		mensionless)
$\omega_{\it m}^L$	Angular velocity of the left motor (rad/s)	N_{cycle}^2	Average load change cycles per hour (dimension-
$egin{array}{c} \omega_m^L \ \omega_m^R \ ec{F}_r \ ec{F}_{res} \ ec{F} \end{array}$	Angular velocity of the right motor (rad/s)		less)
$ec{F}_r$	Rolling resistance force vector (N)	$P_m^L \ P_m^R \ P_{bat}$	Mechanical power of the left motor (W)
$\vec{F_{ros}}$	Resultant force vector (N)	P_m^R	Mechanical power of the right motor (W)
$ec{F}$	Force vector (N)	P_{bat}	Battery power (W)
$ec{v}$	Velocity vector (m/s)	P_{fc}	Net power output of the FC system (W)
ξ_1	Nernst Voltage Coefficient (V)	$P_{friction}$	n Total rolling friction power (W)
ξ_2	Activation Voltage Coefficient (V/K)	$P_{frictio}^{L}$	Rolling friction power for the left wheels (W)
ξ_3	Ohmic Resistance Coefficient (V/K)	P ^L friction P ^R friction	Rolling friction power for the right wheels (W)
ξ ₄	Concentration Voltage Coefficient (dimension-	$P_{H_2}^{fricing}$	Theoretical power supplied by hydrogen (W)
	less)	$P_{motors}^{n_2}$	
a	Geometric length of the FCHAMR (m)	P_{O_2}	Oxygen pressure on the cathode side (Pa)
A_{cell}	Active area (cm ²)	P_{H_2}	Partial pressure of hydrogen on the anode side
b	Axial length of the FCHAMR (m)	2	(Pa)
C_{O_2}	Oxygen concentration (g/L)	$Q_{\it bat}$	Nominal battery capacity (Ah)
E_{aux}	Energy from the auxiliary electronics (Wh)	r	Radius of the FCHAMR's driving wheel (m)
E_{FCHA}	A_{MR} Total requested energy for the FCHAMR	R_1	Internal resistance of the single cell (Ω)
	(Wh)	R_{bat}	Internal resistance of the battery pack (Ω)
$E_{friction}$		SoC	State of charge (dimensionless)
	Kinetic energy (Wh)	T^L	Torque applied to the left motor (Nm)
E_{motors}		T^R	Torque applied to the right motor (Nm)
E_{motors}		T_1	Average low load time per hour (h)
E_{nerst}	Nernst voltage (V)	T_2	Average high efficiency region load operation
F_{II}	Traction force of the FCHAMR (N)		time per hour (h)
F^L	Force applied to the left wheel (N)	T_3	High load operation time per hour (h)
F^R	Force applied to the right wheel (N)	T_{fc}	FC temperature (°C)

U_1	Open circuit voltage of the cell (V)	v_4	Voltage degradation rate under high efficiency
U_{air}	Air utilization (dimensionless)	•	region load $(4.881 \mu V/h)$
U_{fuel}	Fuel utilization (dimensionless)	v_5	Voltage degradation rate under high power load
U_{ocv}	Open circuit voltage of the battery pack (V)		$(11.67\mu V/h)$
v	Linear velocity of the FCHAMR's center of mass	V_t	Average rate of voltage degradation (V/h)
	(m/s)	V_{act}	Activation voltage (V)
v_1	Voltage degradation rate under startup-shutdown	V_{cell}	FC cell voltage (V)
	$(13.79\mu V/cycle)$	V_{conc}	Concentration voltage (V)
v_2	Voltage degradation rate under low load	V_{ohm}	Ohmic voltage (V)
	$(9.42\mu V/h)$	V_{ref}	Nominal reference voltage of the FCHAMR (V)
v_3	Voltage degradation rate under load change	N_{tr}	Transmission ratio (dimensionless)
-	$(0.04234\mu V/kW)$		

CRediT authorship contribution statement

Ghofrane Benarfa: Conceptualization, Methodology, Software, Writing – original draft, Experiment. Ali Ammamou: Conceptualization, Methodology, Reviewing, Editing. Sousso Kelouwani: Conceptualization, Methodology, Supervision, Funding acquisition, Reviewing, Editing. Marie Hébert: Supervision, Reviewing, Editing. Lotfi Zeghmi: Software, Experiment, Reviewing. Samir Jemei: Reviewing, Validation.

Declaration of competing interest

The authors declare that they have no known competing financial interests or personal relationships that could have appeared to influence the work reported in this paper.

Data availability

The authors do not have permission to share data.

Declaration of Generative AI and AI-assisted technologies in the writing process

During the preparation of this work, the corresponding author used ChatGPT in order to improve the language and readability of the manuscript. After using this tool/service, the authors reviewed and edited the content as needed and take full responsibility for the content of the publication.

References

- Arce, A., del Real, A. J., & Bordons, C. (2009). Mpc for battery/fuel cell hybrid vehicles including fuel cell dynamics and battery performance improvement. *Journal of process control*, 19(8), 1289–1304. https://doi.org/https://doi.org/10.1016/j.jprocont.2009.03.004
- Bailey, T., & Durrant-Whyte, H. (2006). Simultaneous localization and mapping (slam): Part ii. *IEEE robotics & automation magazine*, 13(3), 108–117. https://doi.org/10.1109/MRA.2006.1678144
- Bayindir, K. Ç., Gözüküçük, M. A., & Teke, A. (2011). A comprehensive overview of hybrid electric vehicle: Powertrain configurations, powertrain control techniques and electronic control units. Energy conversion and Management, 52(2), 1305–1313. https://doi.org/https://doi.org/10.1016/j.enconman.2010.09.028
- BenChikha, K., Kandidayeni, M., Amamou, A., Kelouwani, S., Agbossou, K., & Abdelghani, A. B. B. (2022). Fuel cell ageing prediction and remaining useful life forecasting. 2022 IEEE Vehicle Power and Propulsion Conference (VPPC), 1–6. https://doi.org/10.1109/VPPC55846.2022.10003313
- Bomze, I. M., & Gabl, M. (2023). Optimization under uncertainty and risk: Quadratic and copositive approaches. *European Journal of Operational Research*, 310(2), 449–476. https://doi.org/https://doi.org/10.1016/j.ejor.2022.11.020
- Chen, H., Pei, P., & Song, M. (2015). Lifetime prediction and the economic lifetime of proton exchange membrane fuel cells. *Applied Energy*, 142, 154–163. https://doi.org/10.1016/j.apenergy.2014.12.062
- Chen, W., Peng, J., Chen, J., Zhou, J., Wei, Z., & Ma, C. (2023). Health-considered energy management strategy for fuel cell hybrid electric vehicle based on improved soft actor critic algorithm adopted with beta policy. *Energy Conversion and Management*, 292, 117362. https://doi.org/https://doi.org/10.1016/j.enconman.2023.117362

- Online health-aware energy management strategy of a fuel cell hybrid autonomous mobile robot under startup-shutdown condition
- Chen, Z., Mi, C. C., Xu, J., Gong, X., & You, C. (2013). Energy management for a power-split plug-in hybrid electric vehicle based on dynamic programming and neural networks. *IEEE Transactions on Vehicular Technology*, 63(4), 1567–1580. https://doi.org/10.1109/TVT.2013. 2287102
- Cheng, S., Hu, D., Hao, D., Yang, Q., Wang, J., Feng, L., & Li, J. (2022). Investigation and analysis of proton exchange membrane fuel cell dynamic response characteristics on hydrogen consumption of fuel cell vehicle. *International Journal of Hydrogen Energy*, 47(35), 15845–15864. https://doi.org/10.1109/ACCESS.2023.3260646
- Eckert, J. J., Barbosa, T. P., Silva, F. L., Roso, V. R., Silva, L. C., & Da Silva, L. A. R. (2022). Optimum fuzzy logic controller applied to a hybrid hydraulic vehicle to minimize fuel consumption and emissions. *Expert Systems with Applications*, 207, 117903. https://doi.org/https://doi.org/10.1016/j.eswa.2022.117903
- Eckert, J. J., Barbosa, T. P., Silva, F. L., Roso, V. R., Silva, L. C., & da Silva, L. A. R. (2022). Optimum fuzzy logic controller applied to a hybrid hydraulic vehicle to minimize fuel consumption and emissions. *Expert Systems with Applications*, 207, 117903. https://doi.org/https://doi.org/10.1016/j.eswa.2022.117903
- Ehsani, M., Gao, Y., Longo, S., & Ebrahimi, K. (2018). Modern electric, hybrid electric, and fuel cell vehicles. https://doi.org/https://doi.org/10. 1201/9780429504884
- Farooq, M. U., Eizad, A., & Bae, H.-K. (2023). Power solutions for autonomous mobile robots: A survey. *Robotics and Autonomous Systems*, 159, 104285. https://doi.org/10.1016/i.robot.2022.104285
- Fayyazi, M., Abdoos, M., Phan, D., Golafrouz, M., Jalili, M., Jazar, R. N., Langari, R., & Khayyam, H. (2023). Real-time self-adaptive q-learning controller for energy management of conventional autonomous vehicles. *Expert Systems with Applications*, 222, 119770. https://doi.org/https://doi.org/10.1016/j.eswa.2023.119770
- Ghobadpour, A., Amamou, A., Kelouwani, S., Zioui, N., & Zeghmi, L. (2020). Impact of powertrain components size and degradation level on the energy management of a hybrid industrial self-guided vehicle. *Energies*, 13(19), 5041. https://doi.org/https://doi.org/10.3390/en13195041
- Graba, M., Amamou, A., Kelouwani, S., Allani, B., Zeghmi, L., Agbossou, K., & Mohammadpour, M. (2023). Toward safer and energy efficient global trajectory planning of self-guided vehicles for material handling system in dynamic environment. *IEEE Access*, 11, 30753–30767. https://doi.org/10.1109/ACCESS.2023.3260646
- Guan, S., Zhuang, Z., Tao, H., Chen, Y., Stojanovic, V., & Paszke, W. (2023). Feedback-aided pd-type iterative learning control for time-varying systems with non-uniform trial lengths. *Transactions of the Institute of Measurement and Control*, 45(11), 2015–2026. https://doi.org/ https://doi.org/10.1177/014233122211425
- He, H., Jia, C., & Li, J. (2022). A new cost-minimizing power-allocating strategy for the hybrid electric bus with fuel cell/battery health-aware control. International Journal of Hydrogen Energy, 47(52), 22147–22164. https://doi.org/https://doi.org/10.1016/j.ijhydene.2022.04.297
- Herrera, V. I., Gaztañaga, H., Milo, A., Saez-de-Ibarra, A., Etxeberria-Otadui, I., & Nieva, T. (2016). Optimal energy management and sizing of a battery-supercapacitor-based light rail vehicle with a multiobjective approach. *IEEE Transactions on Industry Applications*, 52(4), 3367–3377. https://doi.org/10.1109/TIA.2016.2555790
- Hu, H., Yuan, W.-W., Su, M., & Ou, K. (2023). Optimizing fuel economy and durability of hybrid fuel cell electric vehicles using deep reinforcement learning-based energy management systems. *Energy Conversion and Management*, 291, 117288. https://doi.org/https://doi.org/10.1016/j.enconman.2023.117288
- Huang, Y., Hu, H., Tan, J., Lu, C., & Xuan, D. (2023). Deep reinforcement learning based energy management strategy for range extend fuel cell hybrid electric vehicle. *Energy Conversion and Management*, 277, 116678. https://doi.org/https://doi.org/10.1016/j.apenergy.2020. 115460
- Ibrahim, M., Wimmer, G., Jemei, S., & Hissel, D. (2014). Energy management for a fuel cell hybrid electrical vehicle. *IECON 2014-40th Annual Conference of the IEEE Industrial Electronics Society*, 3955–3961. https://doi.org/10.1109/IECON.2014.7049092
- Jordán, J., Palanca, J., Martí, P., & Julian, V. (2022). Electric vehicle charging stations emplacement using genetic algorithms and agent-based simulation. *Expert Systems with Applications*, 197, 116739. https://doi.org/https://doi.org/10.1016/j.eswa.2022.116739
- Kandidayeni, M., Chaoui, H., Boulon, L., & Trovão, J. P. F. (2021). Adaptive parameter identification of a fuel cell system for health-conscious energy management applications. *IEEE Transactions on Intelligent Transportation Systems*, 23(7), 7963–7973. https://doi.org/10.1109/ TITS.2021.3074903
- Li, Q., Yin, L., Yang, H., Wang, T., Qiu, Y., & Chen, W. (2020). Multiobjective optimization and data-driven constraint adaptive predictive control for efficient and stable operation of pemfc system. *IEEE Transactions on Industrial Electronics*, 68(12), 12418–12429. https://doi.org/10.1109/TIE.2020.3040662
- Liu, C., & Liu, L. (2015). Optimal power source sizing of fuel cell hybrid vehicles based on pontryagin's minimum principle. *International journal of hydrogen energy*, 40(26), 8454–8464. https://doi.org/https://doi.org/10.1016/j.ijhydene.2015.04.112
- Madridano, Á., Al-Kaff, A., Martín, D., & De La Escalera, A. (2021). Trajectory planning for multi-robot systems: Methods and applications. *Expert Systems with Applications*, 173, 114660. https://doi.org/https://doi.org/10.1016/j.eswa.2021.114660
- Malviya, A., & Kala, R. (2021). Social robot motion planning using contextual distances observed from 3d human motion tracking. *Expert Systems with Applications*, 184, 115515. https://doi.org/https://doi.org/10.1016/j.eswa.2021.115515
- Martínez, J. S., Mulot, J., Harel, F., Hissel, D., Pera, M.-C., John, R. I., & Amiet, M. (2013a). Experimental validation of a type-2 fuzzy logic controller for energy management in hybrid electrical vehicles. *Engineering Applications of Artificial Intelligence*, 26(7), 1772–1779. https://doi.org/https://doi.org/10.1016/j.engappai.2012.12.008
- Martínez, J. S., Mulot, J., Harel, F., Hissel, D., Pera, M.-C., John, R. I., & Amiet, M. (2013b). Experimental validation of a type-2 fuzzy logic controller for energy management in hybrid electrical vehicles. *Engineering Applications of Artificial Intelligence*, 26(7), 1772–1779. https://doi.org/https://doi.org/10.1016/j.engappai.2012.12.008
- Mattila, J., Ala-Laurinaho, R., Autiosalo, J., Salminen, P., & Tammi, K. (2022). Using digital twin documents to control a smart factory: Simulation approach with ros, gazebo, and twinbase. *Machines*, 10(4), 225. https://doi.org/https://doi.org/10.3390/machines10040225

- Online health-aware energy management strategy of a fuel cell hybrid autonomous mobile robot under startup-shutdown condition
- Meintz, A., & Ferdowsi, M. (2008). Control strategy optimization for a parallel hybrid electric vehicle. 2008 IEEE Vehicle Power and Propulsion Conference, 1–5. https://doi.org/10.1109/VPPC.2008.4677505
- Ming, W., Sun, P., Zhang, Z., Qiu, W., Du, J., Li, X., Zhang, Y., Zhang, G., Liu, K., Wang, Y., et al. (2023). A systematic review of machine learning methods applied to fuel cells in performance evaluation, durability prediction, and application monitoring. *International Journal of Hydrogen Energy*, 48(13), 5197–5228. https://doi.org/https://doi.org/10.1016/j.ijhydene.2022.10.261
- Mohammadpour, M., Kelouwani, S., Gaudreau, M.-A., Allani, B., Zeghmi, L., Amamou, A., & Graba, M. (2022). Energy-efficient local path planning of a self-guided vehicle by considering the load position. *IEEE Access*, 10, 112669–112685. https://doi.org/10.1109/ACCESS. 2022.3216601
- Mohammadpour, M., Kelouwani, S., Gaudreau, M.-A., Zeghmi, L., Amamou, A., Bahmanabadi, H., Allani, B., & Graba, M. (2024). Energy-efficient motion planning of an autonomous forklift using deep neural networks and kinetic model. *Expert Systems with Applications*, 237, 121623. https://doi.org/https://doi.org/10.1016/j.eswa.2023.121623
- Montero-Sousa, J. A., Aláiz-Moretón, H., Quintián, H., González-Ayuso, T., Novais, P., & Calvo-Rolle, J. L. (2020). Hydrogen consumption prediction of a fuel cell based system with a hybrid intelligent approach. *Energy*, 205, 117986. https://doi.org/https://doi.org/10.1016/j.energy.2020.117986
- Poonthalir, G., & Nadarajan, R. (2019). Green vehicle routing problem with queues. Expert Systems with Applications, 138, 112823. https://doi.org/10.1016/j.eswa.2019.112823
- Ravey, A., Blunier, B., & Miraoui, A. (2012). Control strategies for fuel-cell-based hybrid electric vehicles: From offline to online and experimental results. *IEEE transactions on vehicular technology*, 61(6), 2452–2457. https://doi.org/10.1109/TVT.2012.2198680
- Ravey, A., Mohammadi, A., & Bouquain, D. (2015). Control strategy of fuel cell electric vehicle including degradation process. *IECON 2015-41st Annual Conference of the IEEE Industrial Electronics Society*, 003508–003513. https://doi.org/10.1109/IECON.2015.7392644
- Reza, S., Ferreira, M. C., Machado, J., & Tavares, J. M. R. (2022). A multi-head attention-based transformer model for traffic flow forecasting with a comparative analysis to recurrent neural networks. *Expert Systems with Applications*, 202, 117275. https://doi.org/https://doi.org/10.1016/j.eswa.2022.117275
- Rietveld, T., & van Hout, R. (2017). The paired t test and beyond: Recommendations for testing the central tendencies of two paired samples in research on speech, language and hearing pathology. *Journal of communication disorders*, 69, 44–57. https://doi.org/https://doi.org/10. 1016/j.jcomdis.2017.07.002
- Sarma, U., & Ganguly, S. (2020). Design optimisation for component sizing using multi-objective particle swarm optimisation and control of pem fuel cell-battery hybrid energy system for locomotive application. *IET Electrical Systems in Transportation*, 10(1), 52–61. https://doi.org/https://doi.org/10.1049/iet-est.2018.5053
- Song, K., Ding, Y., Hu, X., Xu, H., Wang, Y., & Cao, J. (2021). Degradation adaptive energy management strategy using fuel cell state-of-health for fuel economy improvement of hybrid electric vehicle. *Applied Energy*, 285, 116413. https://doi.org/https://doi.org/10.1016/j.apenergy. 2020.116413
- Stojanović, V. (2023). Fault-tolerant control of a hydraulic servo actuator via adaptive dynamic programming. *Mathematical Modelling and Control*. https://doi.org/10.3934/mmc.2023016
- Sulaiman, N., Hannan, M., Mohamed, A., Ker, P. J., Majlan, E., & Daud, W. W. (2018). Optimization of energy management system for fuel-cell hybrid electric vehicles: Issues and recommendations. Applied energy, 228, 2061–2079. https://doi.org/https://doi.org/10.1016/j. apenergy.2018.07.087
- Sun, P., Song, X., Song, S., & Stojanovic, V. (2023). Composite adaptive finite-time fuzzy control for switched nonlinear systems with preassigned performance. *International Journal of Adaptive Control and Signal Processing*, 37(3), 771–789. https://doi.org/https://doi.org/10.1002/acs_3546
- Takaya, K., Asai, T., Kroumov, V., & Smarandache, F. (2016). Simulation environment for mobile robots testing using ros and gazebo. 2016 20th International Conference on System Theory, Control and Computing (ICSTCC), 96–101. https://doi.org/10.1109/ICSTCC.2016.7790647
- Tian, M., Sang, H., Zou, W., Wang, Y., Miao, M., & Meng, L. (2024). Joint scheduling of agvs and parallel machines in an automated electrode foil production factory. *Expert Systems with Applications*, 238, 122197. https://doi.org/https://doi.org/10.1016/j.eswa.2023.122197
- Tran, D.-D., Vafaeipour, M., El Baghdadi, M., Barrero, R., Van Mierlo, J., & Hegazy, O. (2020). Thorough state-of-the-art analysis of electric and hybrid vehicle powertrains: Topologies and integrated energy management strategies. *Renewable and Sustainable Energy Reviews*, 119, 109596. https://doi.org/10.1016/j.rser.2019.109596
- Troisi, R., & Castaldo, P. (2022). Technical and organizational challenges in the risk management of road infrastructures. *Journal of Risk Research*, 25(6), 791–806. https://doi.org/10.1080/13669877.2022.2028884
- Tsalapati, E., Johnson, C., Jackson, T. W., Jackson, L., Low, D., Davies, B., Mao, L., & West, A. (2021). Enhancing polymer electrolyte membrane fuel cell system diagnostics through semantic modelling. *Expert Systems with Applications*, 163, 113550. https://doi.org/https://doi.org/10.1016/j.eswa.2020.113550
- Vaswani, A., Shazeer, N., Parmar, N., Uszkoreit, J., Jones, L., Gomez, A. N., Kaiser, Ł., & Polosukhin, I. (2017). Attention is all you need. *Advances in neural information processing systems*, 30, 5998–6008.
- Vichard, L., Harel, F., Ravey, A., Venet, P., & Hissel, D. (2020). Degradation prediction of pem fuel cell based on artificial intelligence. *International Journal of Hydrogen Energy*, 45(29), 14953–14963. https://doi.org/https://doi.org/10.1016/j.ijhydene.2020.03.209
- Wang, J., Geng, J., Wang, M., Hu, X., Shao, Z., & Zhang, H. (2022). Quantification on degradation mechanisms of polymer exchange membrane fuel cell cathode catalyst layers during bus and stationary durability test protocols. *Journal of Power Sources*, 521, 230878. https://doi.org/https://doi.org/10.1016/j.jpowsour.2021.230878
- Wang, R., Zhuang, Z., Tao, H., Paszke, W., & Stojanovic, V. (2023). Q-learning based fault estimation and fault tolerant iterative learning control for mimo systems. *ISA transactions*, 142, 123–135. https://doi.org/https://doi.org/10.1016/j.isatra.2023.07.043
- Wang, X., Chen, J., Quan, S., Wang, Y.-X., & He, H. (2020). Hierarchical model predictive control via deep learning vehicle speed predictions for oxygen stoichiometry regulation of fuel cells. *Applied Energy*, 276, 115460.

- Online health-aware energy management strategy of a fuel cell hybrid autonomous mobile robot under startup-shutdown condition
- Wu, Y., Ji, Y., & Gu, F. (2023). Identifying firm-specific technology opportunities in a supply chain: Link prediction analysis in multilayer networks. *Expert Systems with Applications*, 213, 119053. https://doi.org/https://doi.org/10.1016/j.eswa.2022.119053
- Xu, L., Ouyang, M., Li, J., & Yang, F. (2012). Dynamic programming algorithm for minimizing operating cost of a pem fuel cell vehicle. 2012 IEEE International Symposium on Industrial Electronics, 1490–1495. https://doi.org/10.1109/ISIE.2012.6237311
- Yang, B., Lei, Y., Li, X., & Li, N. (2024). Targeted transfer learning through distribution barycenter medium for intelligent fault diagnosis of machines with data decentralization. *Expert Systems with Applications*, 244, 122997. https://doi.org/https://doi.org/10.1016/j.eswa.2023.122997
- Yang, B., Lei, Y., Li, X., Li, N., & Nandi, A. K. (2024). Label recovery and trajectory designable network for transfer fault diagnosis of machines with incorrect annotation. *IEEE/CAA Journal of Automatica Sinica*, 11(4), 932–945. https://doi.org/https://doi.org/10.1109/JAS.2023.124083
- Yavuz, M., Oztaysi, B., Onar, S. C., & Kahraman, C. (2015). Multi-criteria evaluation of alternative-fuel vehicles via a hierarchical hesitant fuzzy linguistic model. *Expert Systems with Applications*, 42(5), 2835–2848. https://doi.org/https://doi.org/10.1016/j.eswa.2014.11.010
- Yu, Y., Wang, G., Tu, Z., Zhan, Z., & Pan, M. (2012). Effect of gas shutoff sequences on the degradation of proton exchange membrane fuel cells with dummy load during startup and shutdown cycles. *Electrochimica acta*, 71, 181–193. https://doi.org/https://doi.org/10.1016/j.electacta.2012.03.141
- Zeng, T., Zhang, C., Zhang, Y., Deng, C., Hao, D., Zhu, Z., Ran, H., & Cao, D. (2021). Optimization-oriented adaptive equivalent consumption minimization strategy based on short-term demand power prediction for fuel cell hybrid vehicle. *Energy*, 227, 120305. https://doi.org/ https://doi.org/10.1016/j.energy.2021.120305
- Zhang, T., Wang, P., Chen, H., & Pei, P. (2018). A review of automotive proton exchange membrane fuel cell degradation under start-stop operating condition. *Applied energy*, 223, 249–262. https://doi.org/https://doi.org/10.1016/j.apenergy.2018.04.049
- Zhao, X., Wang, L., Zhou, Y., Pan, B., Wang, R., Wang, L., & Yan, X. (2022). Energy management strategies for fuel cell hybrid electric vehicles: Classification, comparison, and outlook. Energy Conversion and Management, 270, 116179. https://doi.org/https://doi.org/10.1016/j.enconman.2022.116179
- Zhou, D., Al-Durra, A., Gao, F., Ravey, A., Matraji, I., & Simões, M. G. (2017). Online energy management strategy of fuel cell hybrid electric vehicles based on data fusion approach. *Journal of power sources*, 366, 278–291. https://doi.org/https://doi.org/10.1016/j.jpowsour. 2017.08.107
- Zhou, W., Yang, L., Cai, Y., & Ying, T. (2018). Dynamic programming for new energy vehicles based on their work modes part ii: Fuel cell electric vehicles. *Journal of Power Sources*, 407, 92–104. https://doi.org/https://doi.org/10.1016/j.jpowsour.2018.10.048
- Zhou, Y., Ravey, A., & Péra, M.-C. (2021). Real-time cost-minimization power-allocating strategy via model predictive control for fuel cell hybrid electric vehicles. *Energy Conversion and Management*, 229, 113721. https://doi.org/https://doi.org/10.1016/j.enconman.2020.113721